Cyclic voltammetry evaluation of different anode materials for the electrooxidation of coal dissolved compounds in molten KOH and fuel cell simulation

Sebastián Antonio Cisneros Álvarez

Universidad Nacional de Colombia
Facultad de Minas, Escuela de Procesos y Energía
Medellín, Colombia
2014

Cyclic voltammetry evaluation of different anode materials for the electrooxidation of coal dissolved compounds in molten KOH and fuel cell simulation

Sebastián Antonio Cisneros Álvarez

Thesis work presented as partial requirement for the degree of:
Master of engineering, Chemical Engineering

Advisor:
Msc. Carlos Ignacio Sánchez Sáenz

Research topic:
Electrochemistry
Research group:
Grupo de Investigación en Ingeniería Electroquímica GRIEQUI

Universidad Nacional de Colombia
Facultad de Minas
Medellín, Colombia
2014

Dedicatory

To the "Pachamama", mother of the natural resources that we irrationally consume and destroy

...

Acknowledgement

To my parents and sister for their patience. To Gloria and Marcela for their friendship and "spiritual" help when I exposed the problems that arose during this work. And to Lorena for her tolerance and love.

Abstract

This document shows the results of cyclic voltammetry and fuel cell simulation for the process of electrochemical oxidation of soluble coal compounds in molten KOH. It is shown that nickel and some nickel alloys like inconel 600, chromel and alumel are suitable catalytic materials for this process at the anode. Exchange current densities vary between 28 and 83 A/m^2 and charge transfer coefficients vary between 0.47 and 0.58. Voltammetry experiments also demonstrate that iron alloys, in general, are not suitable for this process because of dissolution of the material. Here voltammetry studies were performed on 410 stainless steel as iron alloy model material. The information obtained after non linear regression analysis to calculate the kinetic parameters for the anodic processes, and that extracted from literature for the cathodic ones, served to solve one proposed model for the continuous steady state operation of a fuel cell for the oxidation of dissolved coal compounds in molten KOH. Comparison of polarization curve and maximum fuel cell power density, obtained by the fuel cell simulation, with those reported by experimental studies show that the proposed model represents the main macroscopic phenomena of this type of systems.
Keywords: Coal, fuel cell, molten KOH, power density, current density, electric potential.

Contents

Symbol list

Latin letter symbols

Symbol	Term	SI unit
a	Surface electrode area per electrode volume	m^{-1}
C	Concentration	$molm^{-3}$
d	Wire diameter	m
D	Diffusivity	m^2s^{-1}
E	Electric potential	V
F	Faraday constant	$96487Cmol^{-1}$
g	Gravity acceleration	ms^{-2}
ΔH	Reaction entalpy	$kJmol^{-1}$
h	Anodic channel height	m
i	Current density	Am^{-2}
I	Total current	A
I	Identity matrix	1
k	Electric conductivity	Sm^{-1}
k	Mass transfer coefficient	ms^{-1}
L	Reactor length	m
l	Reactor width	m
n	Number of transferred electrons or normal unity vector	1
p	Compartment pressure	Pa
P	System Pressure	Pa
Q	Heat	W
R	Volumetric reaction term	$molm^{-3}s^{-1}$

Symbol	Term	SI unit
R	Gas constant	$8.314 \mathrm{Jmol^{-1}K^{-1}}$
Re	Reynolds number	1
Sc	Schmidt number	1
T	Temperature	K
u	Fluid velocity	$\mathrm{ms^{-1}}$
U	Cell voltage	V
V	Electric potential	V
x	Coordinate	m
y	Coordinate	m
z	Coordinate	m

Greek letter symbols

Symbol	Term	SI unit
α	Charge transfer coefficient	1
ϵ	Porosity	1
κ	Permeability	$\mathrm{m^{-2}}$
μ	Dynamic Viscosity	Pas
ν	Kinematic viscosity	$\mathrm{m^2s^{-1}}$
ϕ	Electric potential	V

Subscripts

Subscript	Term
a	Anode
c	Cathode
cell	Cell
cr	Critic

Subscript	Term
e	Electrode
i	Species
in	Inlet
l	Electrolyte phase
m	mass
pol	Polarization
o	Outlet
r	Reaction
s	Solid phase
T	Total

Abbreviations

Abbreviation	Term
^{13}C	Carbon 13
CP/MAS	Cross Polarization Magnetic Angle Spinning
HOMO	Highest Occupied Molecular Orbital
LUMO	Lowest Unoccupied Molecular Orbital
NMR	Nuclear Magnetic Resonance
OCV	Open Circuit Voltage
THF	Tetrahydrofuran

1 Introduction

Direct coal fuel cells are promising devices to produce electric work without the need of a generator and with lesser environmental concerns like noise, particulate material emissions and green gases, like NOx or SOx, production.

The idea to extract electricity from coal is not new. Since finals of XIX century the work of Jaques demonstrated the feasibility of this process, he reported a current density of $100mA/cm^2$ and a voltage close to $1V$ by using graphite rods as anodes [17]. However, the electrolyte degradation and the contamination of the media by non volatile species made this process difficult to perform [45].

It has been demonstrated [33] the possibility of oxidizing solid biocarbon coal in a fuel cell, but the results show a very little promising and interesting application because of the low power generation. The best result was near $19mW/g$ for a process which needs temperature above $200^{\circ}C$ and a an operating pressure close to $36bar$. In another work [44] the performance of a direct carbon fuel cell in molten hydroxide was evaluated using graphite as anode and it was obtained a maximum power density of $57mW/cm^2$ at approximately $250mA/cm^2$, polarization curves showed a high influence of ohmic losses attributed to inter electrode electrode spacing. Despite the relative high current density obtained, it is little pragmatic to use graphite as anode because it is not an abundant natural material, this fuel could be expensive and not a global one.

Other research activities have been performed by using molten carbonate media. There is a great work of many research groups and various publications elsewhere, however one of the most complete works [9] reported a study of different carbonaceous materials as anodes for the electrooxidation process at around $600^{\circ}C$ and power densities as high as $84mW/cm^2$. However, most of these evaluated materials must be pretreated before the electrochemical process and operating conditions reveal difficult to continuously feed coal particles and a high corrosive media.

Despite the mentioned difficulties, in this work it is tried to demonstrate the possibility to develop an electrochemical device that can be used as a fuel cell which can extract electrical energy from dissolved coal molecules, which could be easier to construct and control than the anterior attempts. Also, it is tried to suppose and explain some possibly electrochemical

reactions based on the organic chemistry and electro-organic chemistry theory taking as a base the knowledge and development of coal molecular models that identify the principal functional groups that compose this material. Also, the main electrochemical parameters to describe the kinectic behaviour of the fuel cell anode like exchange current density and symmetry factors are reported and used in the simulation calculations.

The interest in this work is not to elucidate the structure of the coal type that is used in the investigation neither to confirm their reaction mechanisms in the media because it is far of our possibilities to access to most of the experimental techniques required for do it. In addition, a rigorous theoretical approach to these phenomena would deviate the investigation objectives, but this is not an apologize because it is known that a deeper knowledge is needed to gain a closer approximation to the understanding of the phenomena involved in this kind of processes and for this reason it is emphasized along the document about the key aspects that open important questions about the physics and chemistry of the process like coal molecular interactions, the relationship between coal type an its reactivity and functional groups effects. Also it is tried to refer the reader to adequate documentation for those research areas.

2 The importance of coal molecular structure

Recognizing and identifying the main molecular structure properties of coal is the first step to understand and predict the principal phenomena that arise when it is subjected to any process. The following is a summary of a bibliographic research concerning to the developing of coal molecular models and its importance for the comprehension of the principal macroscopic behaviours identified in this work.

As coal has been found to be a very important material for humanity development it has been necessary its understanding. It could be said that two approaches to analyse coal exist. By one hand, is the approach that makes use of chemical techniques or analyses based on spectra, that can be invasive or non invasive, to determine coal constitution. By the other hand, is the approximation by theoretical analyses based on different types of interactions at molecular scale and that require some experimental information to program the algorithms that give the equilibria molecular representations of different kinds of coals. However, both approaches are complementary, as will be explained in the following paragraphs.

Before entering in the analyses of different approaches to study coal, one general idea about what it is can be constructed having the following in mind: coal is chemically and physically a heterogeneous material composed by organic and inorganic compounds. The former are divided in maceral groups classified according to their chemical composition and are known as exinite, vitrinite and inertinite. In the table **2-1** this classification is shown.

Table **2-1**: Coal maceral groups

Maceral group	Atomic carbon content	H/C Atomic ratio	Volatile content
Exinite	43-62%	1.18-0.59	79-18%
Vitrinite	51-62%	0.8-0.6	40-18%
Inertinite	59-67%	0.64-0.47	31-11%

Source S.C.Tsai. Coal Science and Technology Fundamentals of Coal Benefication and Utilization. 1982. Amsterdam. Elsevier. 1 st Edition. Chapter 1.

Vitrinite has been found to be richer in polar groups than exinite which has been characterized for its high amount of aliphatic groups. For vitrinite rich coals it can be said that polar interactions are the most important for its energetic features while for exinite rich coals, hydrogen bonding interactions dominate its energetic behaviour. Inertinite, by the other hand, is characterized by a high amount of condensed aromatic rings and the lowest hydrogen to carbon and oxygen to carbon ratios and another type of phenomena, like $\pi - \pi$ interactions, could have a more important role than dipole-dipole and hydrogen bonding. With this information it could be a little easier to understand the complexity of this material.

2.1 Experimental analyses

This approach is based on the results obtained by techniques that require the estimation of coal constituents concentration. Many times, this is done by invasive methods and often destruction of the solid structure occurs. Because of this disadvantage, care must be taken because not always the results obtained by one technique match when compared to another results detected by different means. For example, in [16] it was found that the contribution of aliphatic fragments to coalified wood was around 33% according to pyrolysis analyses and this contribution was attributed principally to n-alkane/alkene fragments. But, NMR spectra did not detect signals corresponding to this type of components. The answer is that, by subjecting coal to pyrolysis, chemical changes took place and the components detected after the treatment not were the same as the original existing in the solid before the treatment. However, this type of analyses complemented by other techniques give a lot of information that has been very useful to describing coal molecular structure and are the feed to the computer programs that calculate the interactions and construct the molecular models.

In [35] a three dimensional network for representing coal was developed using a Montecarlo algorithm which employed the probability density functions for 26 structural groups whose concentrations were calculated from data of CP/MAS ^{13}C NMR, flash pyrolysis, elemental analysis, proton NMR and chemical functional group analysis. This network consisted in two phases, a mobile and a rigid one. The first one was composed of small linear molecules bonded to the solid coal macro structure and the second consisted in highly cross linked covalently bonded structure. A reaction propagation algorithm for 1450 reactions that enclosed initiation, hydrogen abstraction, β scission, radical addition, radical disproportionation and radical recombination reactions was developed. It was reported that hydrogen abstraction reactions dominated the initial reactions due to the high initial hydrogen concentration distributed between aromatic rings and functional groups principally. This observation serves as an indicative that it is possible to affect coal structure by utilizing groups which can extract protons from molecules which can be stabilized by resonance or charge distribution on hetero atoms.

In [11] one group of researchers published some results, very pertinent to the discussion of the molecular structure of coal that existed in the 80's decade. Two of these communications reported information that corroborates in great manner the results supported by theoretical analyses, next section. In the first short communication of this publication it was mentioned that molecular structures related to compounds with different number of aromatic groups attached to short alkyl chains could be part of a low rank bituminous coal. The affirmation was supported by Py.f.i.m.s (Pyrolysis field ionization mass spectroscopy). These components were proposed to have two, three, four or five aromatic groups attached by alkyl substituents of maximum 8 carbons. Results indicated that long alkyl compounds are not abundant in coal. In the second short communication of the same publication an analysis of the THF soluble fraction obtained from a subbituminous coal extracted by Potassium-crown-ether reagent (K-CE) suggested poly-methylene groups as the major aliphatic component of coal and that under alkaline conditions the polar groups of coal are present in salt form ($-O^-M^+$) and if the groups are sufficiently acids, these salts could be converted from $-O^-M^+$ to OH, which is THF extractable, according to the results published. These THF extracts were found, by infrared, to be dominated by sharp C-H stretching vibrations below $3000cm^{-1}$, which is an indicative of the aliphatic character of that extracts fragments. Also, the extracts showed O-H stretching vibrations in the range of $3400 - 3200cm^{-1}$ which is an indicative that the aliphatic components should be attached to the hydroxyaromatic ring system.

2.2 Theoretical analyses

Experimental techniques permit to identify coal constituents and various of their main characteristics. This data could obtained from different analysis procedures like elemental analyses, functional group analyses, ^1H and ^13CNMR, flash pyrolysis coupled with gas chromatography and mass spectroscopy (flash pyrolysis/GC/MS) among others. But, the thermodynamic aspects that serve to explain which are the physically and chemically facts that conduce to a determined behaviour require theoretical fundamentals. The construction of molecular structures from analytical data is known as CASE (Computer Aided Structure Elucidation) [15]. With these techniques, structural molecular models can be build by the input to the software of the qualitative and quantitative information obtained from various of the mentioned analyses. However, by one hand, too large number of representations are possible and it is hard to select a representative one of all models and, by the other hand, building all the possible models obtained, even for a single maceral, would be tedious. At this stage, techniques like the SIGNATURE program [15], which are able to calculate the number of possible models and build a representative sample of models, could be very helpful to obtain an average representation for a macromolecule. Once a group of representations is calculated, these molecular models must be evaluated at equilibrium to corroborate the

accuracy of the model by determining a physical parameter for which experimental data are available, like true density or porosity. At this point Molecular Dynamics, Montecarlo simulations, molecular orbital theory and quantum mechanics become very useful to obtain answers to the questions that are formulated to the respect. This modelling approach uses techniques for calculating the minimum potential energy that molecules adopt in solid carbon when it is at equilibrium before or after subjecting it to any process.

More than 134 molecular representations of coal have been proposed between 1942 and 2010. A major part of these models belong to bituminous coals, but efforts have been made to elucidate also the molecular structure of anthracite, lignite and subituminous coals. First attempts were related to the modelling of structures that were in accordance with reactivity for processes like liquefaction and these representations were made by hand and corroborated by chemical analysis of both, parent coal and the products obtained after the processes. Although good models were obtained [39] it was recognized that $3D$ representations were needed to have a better approach that were in accordance with physic features exhibited when coals were subjected to another processes like drying, dissolution or combustion. Fortunately, as computer techniques and computation power have advanced through the years great achievements in this area have been possible.

Average representations of coal consist on clusters of three or four fused aromatic rings substituted with heteroatoms and short chain aliphatic groups and interconnected by hydroaromatic, etheric or short aliphatic linkages. A major part of coal molecular models are small scale, < 5000 atoms, and their application for exploring structure-property and structure-behaviour relationships of coal are limited [8]. To obtain a deeper knowledge about these aspects it is necessary to incorporate structural diversity and it means large scale molecular models.

These calculations include energetic contributions which have been divided as bonding and non bonding contributions as shown in the figure **2-1**.

The equation 2-1 shows the calculation for the total energy performed by the simulations.

$$E = (E_{stretch} + E_{bend} + E_{torsion} + E_{inversion}) + (E_{vw} + E_{electrostatic} + E_{hydrogen}) \tag{2-1}$$

Van der Waals interactions have been recognized as very important to the formation and stabilization of coal macromolecular structure [7], [29]. However, calculations by using DREIDING force field [7] served to demonstrate that hydrogen bond interactions are more important for low rank coals than are Van der Waals interactions, that could be more important as coal rank increases.

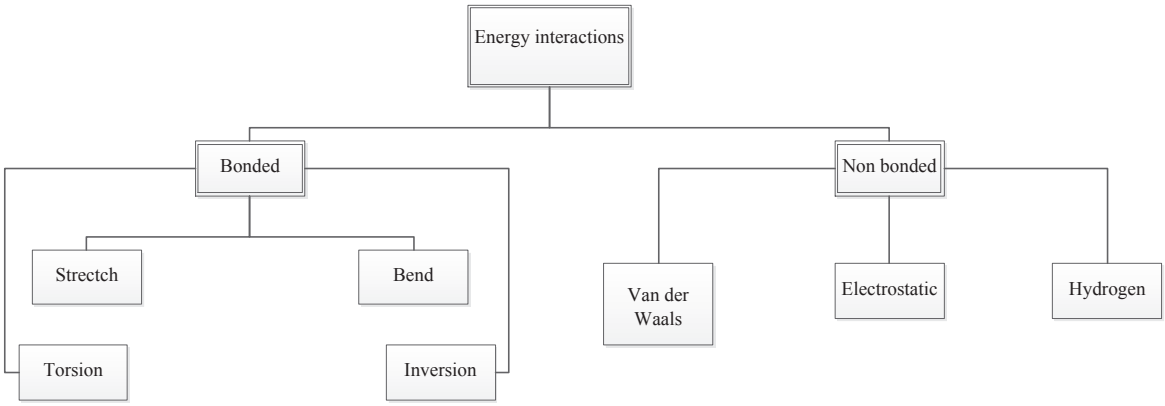

Figure **2-1**: Energy contributions to the calculation of coal molecules potential energy

To continue on the same line of hydrogen interactions importance, in [41] it is reported that hydrogen bonds and aromatic-aromatic interactions form strongly associated structures and the disruption of one interaction site does not imply disruption of all the associated structure and that explains why not all the potentially extractable material can be extracted from coal and that is because of the possible effect of stabilization that Van der Waals interactions have. In this publication it was also found that hydroxyl groups are the dominating hydrogen bond donors and that they can strongly interact with hydrogen bonding solvents, those that available electrons in the most electronegative atom, disrupting coal-coal bond interactions affecting hydrogen bonding distribution in the coal matrix. This fact corroborates that hydrogen extraction by the solvent is possible if the solvent has any group with sufficient affinity to achieve the proton abstraction.The types of associated OH groups are summarized in table 2.2.

Table **2-2**: Type of associated OH groups in coal

Free OH groups
OH-π hydrogen bonds
Self associated OH-OH bonds
OH-ether hydrogen bonds
Cyclic OH groups
OH-N acid base structures

The importance of $\pi - \pi$ hydrogen and electrostatic interactions is mentioned in [42] in which only a rough estimation of the experimental extraction yield was obtained from simulation

calculations, presumably because these interaction types were not taken into account. However it was also remarked the importance of other phenomena like transport limitations of extractable material from solid coal and molecular entlagement, but these other phenomena could be related with electrostatics and hydrogen interactions.

Hetero atoms have also an important role in coal molecular behaviour, although their concentration has been reported as a small fraction of coal composition: 1-3.5% distributed among all the molecules comprising the coal structure, almost for bituminous coal types [25]. Because of its presence, aromatic structures present small HOMO-LUMO gaps and the main consequence is that Van der Waals interactions become stronger [32]. An indicative of the strength of this forces is evidenced in [29] where the calculated values for the density were lower than the experimental reported for coals. This was attributed, in part, to the lack of heteroatomic moieties which were found to be very important to electrostatic interactions by dipoles and induced dipoles effects.

In [40] it was found by Molecular Dynamics simulation that there are cooperative interactions in coal, attributed to non-bonding interactions, mainly to hydrogen bonds and aromatic-aromatic interactions (Van der Waals forces), that prevent the breaking of coal associates when it is subjected to a dissolution process with solvents like methanol and benzene. When coal is in contact with solvents, some bonds of the solid structure disrupt, but the presence of Van der Waals and hydrogen bonding interactions balance the disruption occurred in the sections where the solvent attacks and no total coal dissolution is observed. However, when coal is in contact with solvents in which structure are present atoms like nitrogen, as in the case of pyridine, dissociation of the molecular matter is appreciably because hydrogen bonds and aromatic-aromatic interactions are disrupted by the electrostatic attractions that take place thanks to the partially negative charge of the nitrogen atoms.

Although this strategy has been very successful for explaining tendencies of coal solubility and extraction ,it is important to say that DREIDING force field and, in general, the calculations of Molecular Dynamics or Montecarlo techniques usually reported in coal molecular modelling papers have not taken into account interactions like stretch-bend, atomic dipoles which could be important for understanding the behaviour of coal in processes which include complex fluids.

From the preceding discussion, it can be concluded that hydrogen bonding and Van der Waals interactions are the most important energetic contributors to coal structure and that a lot of macroscopic observations could be explained as functions of these two kinds of non-bonding interactions and that, atoms with unpaired electrons interact strongly with hydrogen and coal polar functional groups, this coal-solvent interaction, depending on the nature of the solvent, could have sufficient strength to destruct associative intra and intermolecular coal

forces and soluble coal compounds could be obtained when treating it with appropriate solvents. These arguments will be used to explain the fundamentals of the chemistry and the experimental observations that are the contents of the next chapters.

3 Fundamental chemistry of the process

One of the main attempts to explain the mechanisms of electro oxidation of coals is reported in [38] where it is proposed that electrolytically produced inorganic radicals from water decomposition should be the responsible of the anthracite oxidation in a coal fuel cell. It is argued that organic compounds are oxidized according to a mechanism of aromatic ring opening by hydrogen abstraction from active sites by the unstable radicals and a further attack by oxygen molecules generating carboxylic acids as the final oxidation product.The chemistry of radicals is complex and it is known that the mean life of these species is short and that is the reason because it was proposed that the coal must to be in contact with the electronic conductor to achieve its electro oxidation. Following is showed the possible reactions that include radicals proposed in [38].

$$OH^- \rightarrow OH^{\cdot} + e^- \tag{3-1}$$

$$2\,OH^{\cdot} \rightarrow [H_2O_2] \rightarrow O_2 + 2\,H^+ + 2\,e^- \tag{3-2}$$

$$4\,OH^{\cdot} \rightarrow [{}_2H_2O_2] \rightarrow 2\,H_2O + O_2 \tag{3-3}$$

$$H_2O_2 + OH^- \rightarrow H_2O + HO_2^- \tag{3-4}$$

$$HO_2^- \rightarrow HO_2^{\cdot} + e^- \tag{3-5}$$

$$HO_2^{\cdot} + OH^- \rightarrow H_2O + O_2^- \tag{3-6}$$

$$O_2^- \rightarrow O_2 + e^- \tag{3-7}$$

Another identified homogeneous reactions of radicals are the following.

$$OH^{\cdot} + OH^{\cdot} \rightarrow H_2O_2 \tag{3-8}$$

$$2\,OH^{\cdot} + H_2O \rightarrow H_2O + 2\,HO_2^{\cdot} \tag{3-9}$$

$$OH^{\cdot} + HO_2^{\cdot} \rightarrow H_2O + O_2 \tag{3-10}$$

$$HO_2^{\cdot} + HO_2^{\cdot} \rightarrow H_2O + O_2 \tag{3-11}$$

With the following values for the respectively reaction coefficients: $6*10^9$, $4.5*10^7$, $1.5*10^{10}$ and $2.5*10^6\ M^{-1}s^{-1}$.

Although the mentioned study set some bases for this kind of processes it is important to highlight that anthracite did not dissolved in the media used for the experimentation. For the case studied in this thesis coal was dissolved and for this reason the chemistry of the process must be different in some aspects that will be explained in the next lines.

In [23] it was found that treatment of coal particles in concentrated alkaline solutions with oxygen could result in the production of humic acids, which are alkali soluble compounds, by reactions probably involving a base catalysed mechanism accompanied by initiation, propagation and termination steps which could include radical organic reactions as shown by equations 3-12 to 3-16. The rate controlling steps were identified to be 3-13 and 3-15. Both imply charge transfers.

$$R{-}H + B^- \rightarrow R^- + B{-}H \tag{3-12}$$

$$R^- + O_2 \rightarrow R^{\cdot} + O_2^{\cdot -} \tag{3-13}$$

$$R^{\cdot} + O_2 \rightarrow R{-}O{-}O^{\cdot} \tag{3-14}$$

$$R{-}O{-}O^{\cdot} + R^{-} \rightarrow R^{\cdot} + R{-}O{-}O^{-} \tag{3-15}$$

$$R{-}O{-}O^{-} + B{-}H \rightarrow B^{-} + R{-}O{-}O{-}H \tag{3-16}$$

Although, the reaction conditions of these experiments where not sufficiently strong to dissolve coal in a short time period, a piece of coal could be consumed in several months according to their kinetic results and this could permit to speculate about some mechanisms similar to that base catalysed one to have an idea about what happens in the molten alkaline media used in this work.

Abundance of acidic functional groups in low rank coals give place to coulombic forces, acid groups such as -COOH and -OH are partially ionized and interact with cations such as R_3^+H, Ca^{2+} and Na^+ [31] and this could be an explanation of the behaviour observed related with the coal dissolution and the hypothesis that there is an acid-base relationship between coal and potassium hydroxide. It is possible to speculate about some reactions of the main organic groups present in coal, as stated in chapter 2. Here, in particular, four distinct speculated mechanisms of reaction are used to explain how could hydroxide groups attack some coal functional groups and which steps could be related with electron transfer reactions. The main reason to do this is to show that, contrary to direct coal fuel cells with molten carbonate media, the cell reaction in this molten potassium hydroxide media is not as simple as that reported elsewhere ([9], [6], [21], [34]) between carbon and oxygen to produce carbon dioxide, reaction 3-17. Coal functional groups, in particular the acidic ones, should be the reactive organic species from which electricity can be obtained as reported in [24].

$$C + O_2 \rightarrow CO_2 \tag{3-17}$$

The supposed reactions involve a phenolic alcohol, a carboxylic acid and a cyclic ketone. These groups have been identified for sub-bituminous coal and the reactive molecules have been chosen only to demonstrate the possibility of how electrical energy can be obtained from the oxidation of the organic matter, but it must be clear that the existence of these type of compounds was not evaluated in this work and perhaps thousands of different reactions that include as complex processes as free radical reactions of macromolecules are possible.

All the mechanisms show a supposed route to the production of CO_2, H_2O and electrons from the starting reduced organic molecule. It is known that the oxidation of these kind of molecules involves a large set of complex steps, take as an example the mechanisms for glucose oxidation by molecular oxygen.

One mechanism for the reduction reaction at the cathode is also supposed, based on the possibility of the existence of the oxide ion species in molten media [37], [1]. However, a mechanism for oxygen reduction in this media is yet unknown.

By summing both supposed semi-reactions, for the organic molecule oxidation and for the oxygen reduction, a global reaction which represents one possible cell reaction is obtained and, by evaluation of thermodynamic data, the enthalpy of the reaction could be evaluated. Particularly, and because of the lack and the scatter character of these data at the temperature of the experiments, only the enthalpy for the reaction of the aromatic alcohol has been estimated, but the procedure should be the same for other reactions.

Phenolic alcohol speculated reaction mechanism

In the figure 3 is shown the speculated mechanism for an aromatic primary alcohol, with R being an isopropyl group.

The semi-reaction for this mechanism can be written as follows

$$\mathrm{C_{10}H_{14}O + 6\,OH^- \rightarrow 2\,H_2O + CO_2 + C_9H_{16}O_3 + 6\,e^-} \tag{3-18}$$

It is of primary importance to highlight that the produced organic compounds should continue reacting until all organic matter is transformed to water and carbon dioxide following a lot of possible mechamims, but studying these aspects is not considered part of the objectives of this thesis.

Oxygen reduction speculated reaction mechanism

$$\mathrm{\frac{1}{2}O_2 + 2\,e^- \rightleftharpoons O^{2-}} \tag{3-19}$$

$$\mathrm{O^{2-} + H_2O \rightleftharpoons 2\,OH^-} \tag{3-20}$$

By summing reactions 3-19 and 3-20 the next semi-reaction can be obtained

$$\frac{1}{2}O_2 + 2\,e^- + H_2O \rightleftharpoons 2\,OH^- \tag{3-21}$$

By summing the reactions 3-18 and 3-21 the global reaction is as follows

$$C_{10}H_{14}O + \frac{3}{2}O_2 + H_2O \rightarrow CO_2 + C_9H_{16}O_3 \tag{3-22}$$

Both semi reactions have been attributed to a fem value evaluated by the knowledge of the standard formation enthalpies of the participating species and their respective heat capacities calculated at the reaction conditions and supposing that reaction free Gibbs energy could be approximated to reaction enthalpy.

Data to estimate standard formation enthalpies and heat capacities were extracted from [12] and NIST data bases.

The estimated fem for semi-reaction 3-18 have a value of 0.927 volts with a reaction enthalpy of $-537.2 kJ/mol$. For semi-reaction 3-21 the respective values were estimated in 0.747 volts and $-144.3 kJ/mol$ at 523 K and 1 atm. The total reaction enthalpy was estimated to be approximately $-440 kJ/mol$ With this calculations it is possible to say that, if 3-22 were true a fem value for it were proximately 1.7 volts. In the next chapter, it will be seen that this value reduces because of kinetic limitations.

Following are shown the speculated mechanisms for a carboxylic acid and a cyclic ketone, but again it is mentioned that these are only speculative reaction routes which could be only a little fraction of the thousands of reactions that could exist in this system.

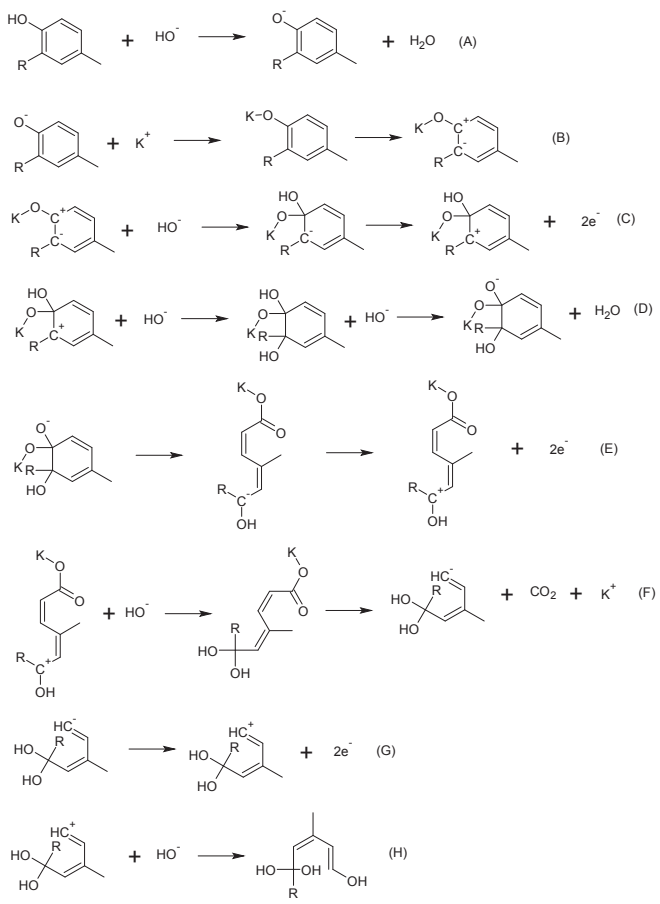

Figure **3-1**: Speculated reaction mechanism for a phenolic alcoholic group

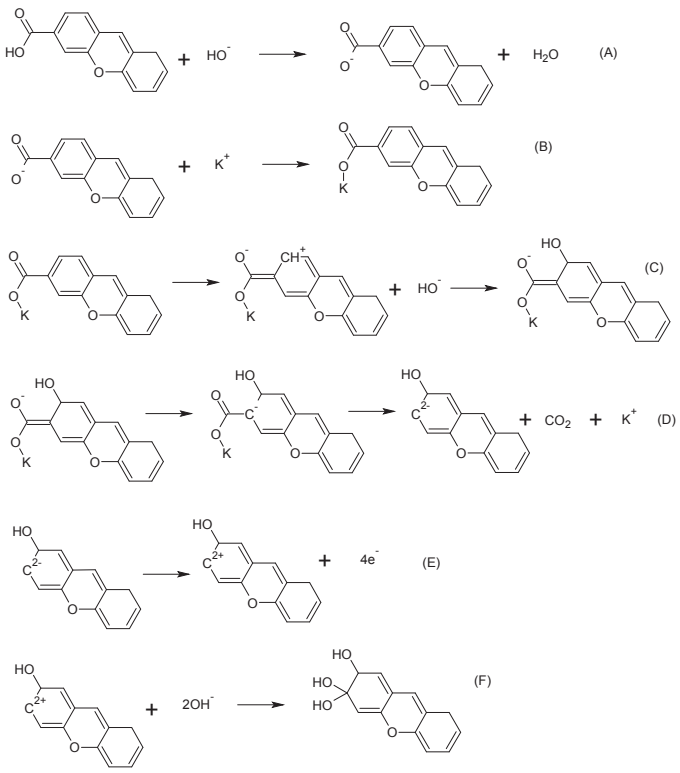

Figure **3-2**: Speculated reaction mechanism 1 proposed for carboxylic acid groups

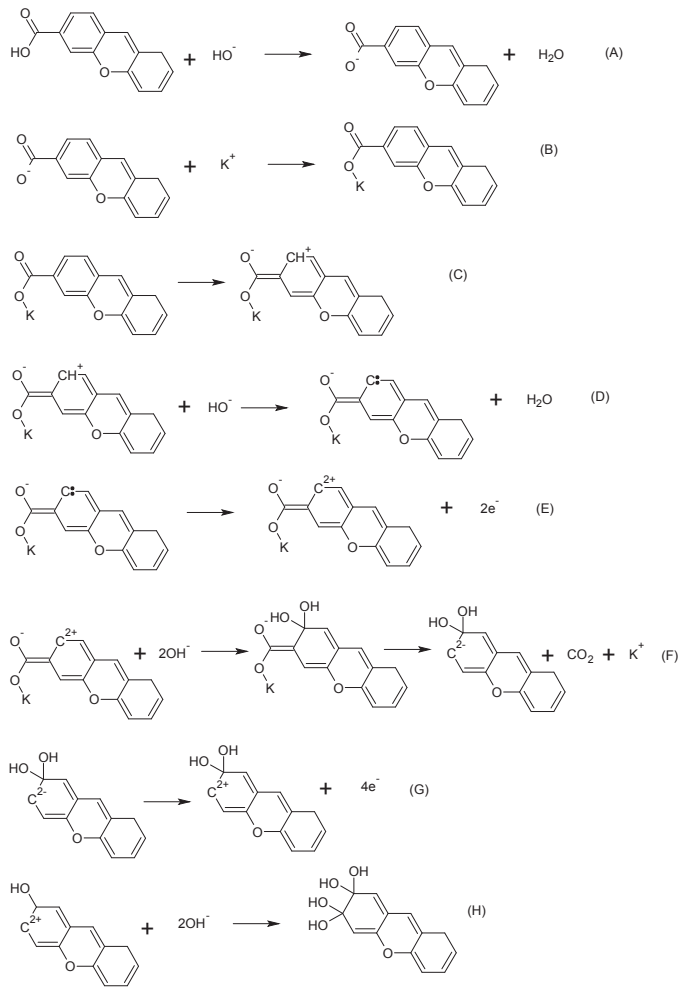

Figure **3-3**: Speculated reaction mechanism 2 proposed for carboxylic acid groups

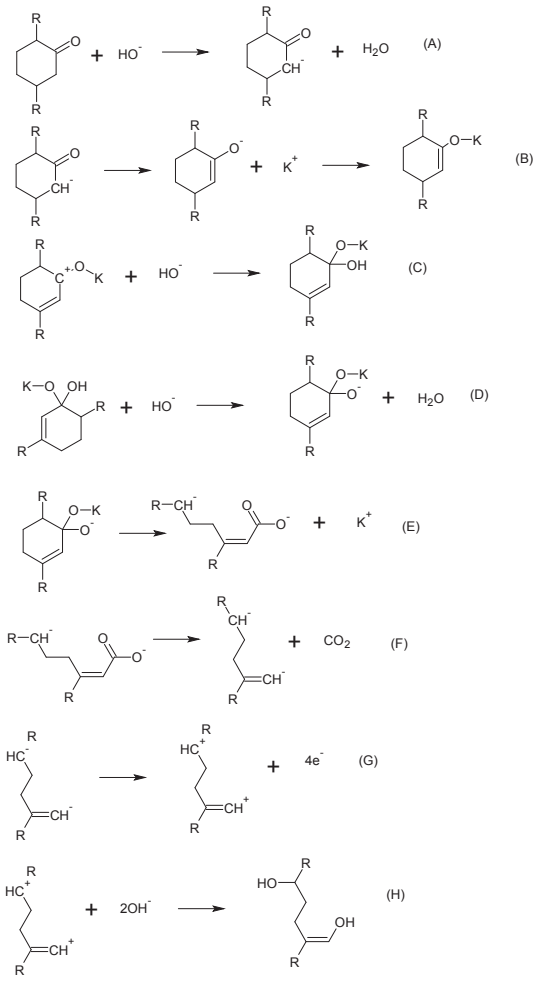

Figure **3-4**: Speculated reaction mechanism proposed for a cyclic ketone group

4 Experimental

When coal is added to the melt it is dissolved following different reaction paths depending on the chemical nature of the organic matrix, as stated in the previous chapters. As seen in the chapter 2, thermal disruption of intercluster interactions and hydrogen bonds influences the dissolution and extractability of coal compounds, however also the force of an hydrogen acceptor is a factor of great importance because this gives place to charged species and polar interactions arise and the force of these interactions has been shown to be the most important in the physics and chemistry of coal behaviour.

Treatment of coal by alkali solutions is not new and works have been published in which coal dissolution have been reported. For example in [2] is referenced the work of Fischer and Schrader in which is reported that 21% of coal was dissolved by treatment with 4.1N KOH at 300^oC. This quantity can be enhanced by increasing residence time, alkali concentration or decreasing particle size. This last effect is maybe related with the fact that diffusion controls the process for the type of coal treated. By knowing these aspects the experimentation was made with melted KOH, a coal with possibly a great amount of functional groups and a working electrode with a sufficient catalytic activity to oxidizing organic molecules.

Reactive grade KOH supplied by Merck, without any posterior treatment, and coal with the proximate and elemental analysis shown in tables **4-1** and **4-2**, respectively, have been used to prepare the blanks and the working melts. Coal was ground in a ceramic mortar to a mean particle size approximate to 1 mm. The solid was previously washed to remove mine sludge, but were not subjected to drying processes other than exposure to air and sun. Also no ash removing pretreatments were carried out because it is important to know if the process can be achieved with coal directly from mines without the implementation of intermediate processes before the fuel cell.

Figure **4-1** shows an scheme of the experimental set-up.

All the electrodes were polished to 1200 grade sand paper and after this treatment were submerged in 65% per weight HNO_3 during approximately 10 seconds and then washed with distilled water to remove nitrate traces.

The electrodes were introduced into alumina tubes provided by *Omega*® company with the

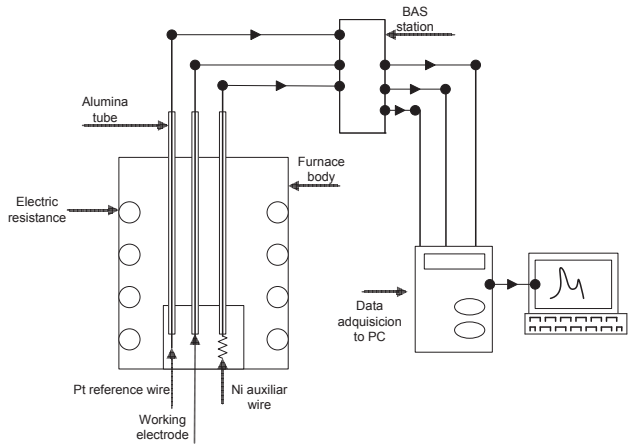

Figure **4-1**: Scheme of the experimental set-up

Table **4-1**: Coal proximate analysis

Property	Percentage
Moisture	3.87
Volatile matter	46.25
Fixed carbon	46.54
Ash	3.33

specification Omegatite® 450 reference ORX-11618 which chemical composition is given in table **4-3**. This was done to obtain a fixed exposed electrode area and to insulate the metals to avoid short circuit with the metal from the exterior body of the furnace.

The potential sweeps were carried out in a BAS100W station at different sweep rates ranging from $20mV/s$ to $200mV/s$ with a sensivity between $100mA/V$ and $10mA/V$. These relatively high values were needed because of equipment saturation due to the high currents obtained during the process.

Heating process was carried out in a furnace provided by *Industrias Terrígeno* with a ramp of approximately 5^oC per second until reaching the experimental temperature of 250^oC. The container was a quartz crucible which was inert to both, the KOH melt and the KOH-dissolved coal mixture.

Table **4-2**: Coal elemental analysis

Element	Percentage
C	59.04
H	5.75
N	1.56

Table **4-3**: Omegatite® 450 tube specifications

Compound	Percentage
Al_2O_3	99.8
SiO_2	0.070
MgO	0.050
Na_2O	0.005
Ca	0.03
Fe_2O_3	0.025
Cr_2O_3	<0.003
TiO_2	0.004
MnO	0.001

4.1 Cyclic voltammetry studies for different materials

4.1.1 Nickel

Nickel has been used as catalyst for the electrochemical oxidation of organic compounds because its oxidized states have been found to promote electron transfer and enhacement of oxygen evolution reaction OER at high anodic potentials. By observing Pourbaix diagrams [5] it could be seen that stable nickel oxidized species at high temperatures and pH could be either oxides, hydroxides or oxyhydroxides. The former has been attributed to be NiO known as businite while the later have been designated as NiOOH which could exist in two different forms, depending on media and process conditions, as β or γ phase, but presumably large ionic radii alkaline cations facilitate the existence of the latter phase [5].

Nickel oxide and oxyhydroxide has been identified by XRD analyses after passivating nickel surfaces by applying potential sweeps in anodic directions [14]. It was proposed [43] that

the passive film formed on nickel surface is composed by an inner NiO film and an outer film which could be $Ni(OH)_2$ or NiOOH depending on the ambient conditions. This double film morphology was found by [26] by using Electrochemical Impedance Spectroscopy on Fe electrodes at a pH close to 14. A characteristic of the system is that two kinetic constants can be identified, which is an indicative of the different physic and chemical nature of both layers.

According to the anterior discussion, the passivated nickel electrode surface was probably composed by two layers which could favour different reaction paths for the present species.

By observing figure **4-2** it is clear that oxidation processes were identified as A1 and A2, as shown in figure 4.1.1. The main aspect of these processes is their width. This occurs because probably different reactions take place at very similar potentials in this range. Process A2 could be related with reactions 4-1 to 4-4. These reactions involve the production of nickel hydroxides which could be oxidized at more anodic potentials to nickel oxyhydroxides as stated in reaction 4-5 before oxygen evolution.

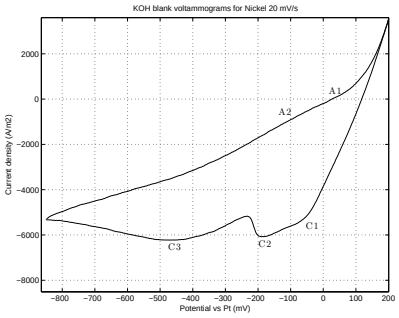

(a) KOH blank voltammogram on nickel at $20mV/s$

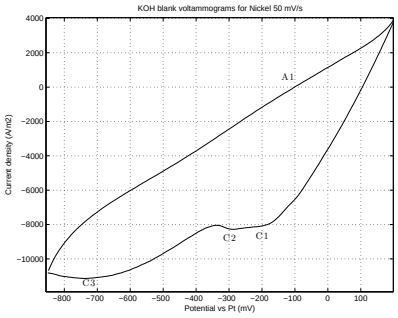

(b) KOH blank voltammogram on nickel at $50mV/s$

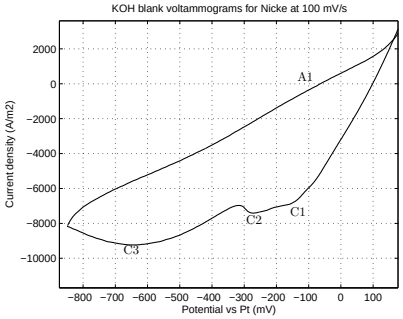

(c) KOH blank voltammogram on nickel at $100mV/s$

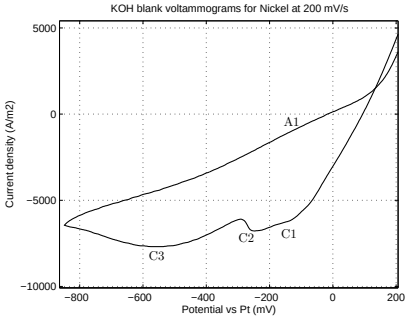

(d) KOH blank voltammogram on nickel at $200mV/s$

Figure **4-2**: Blank voltammograms using nickel as electrode

$$Ni + 2OH^- \rightleftharpoons NiO + H_2O + 2e^- \tag{4-1}$$

$$Ni + 2OH^- \rightleftharpoons Ni(OH)_2 + 2e^- \tag{4-2}$$

$$Ni(OH)_2 + OH^- \rightarrow Ni(OH)_3^- \tag{4-3}$$

$$Ni(OH)_3^- \rightleftharpoons Ni(OH)_2 + e^- \tag{4-4}$$

The existence of the anionic species could be corroborated in Pourbaix diagrams reported by [5] at high pH and potentials and at temperatures above $100^{\circ}C$.

The reaction of oxhyhydroxide formation is reversible and its corresponding reduction peak could be attributed to peak C1. The existence of this species has been confirmed by XRD analyses and cyclic voltammetry after nickel nano particles passivation and it was found to be a catalytic mediator for the electrochemical oxidation of formic acid as reported by [19] and [13]. The produced nickel hydroxide from the reverse reaction of reaction 4-5 could be reduced to metallic nickel by the reversible process of reaction 4-2 which is attributed to process C2. Because of the presence of oxidizing agents the metal is quickly passivated and that is the reason because current density increases after this process. Then, at more cathodic potentials the process C3 arises and could be related with the reversible parts of reactions 4-1 to 4-4.

$$Ni(OH)_2 + OH^- \rightleftharpoons NiOOH + H_2O + e^- \tag{4-5}$$

In figure **4-3** are shown the voltammograms for the Coal-KOH mixture at different potential sweeps. It is clear that pH decreases because of the coal moisture. First, it can be seen a process named C1' in the range between $10mV/s$ to $50mV/s$ which reaches a local minimum and then is followed by an oxidation process which precedes a strong cathodic current density. This peak could be related with nickel restoration reactions represented by the reversible processes of reactions 4-1 and 4-2. The high cathodic current is associated with hydrogen evolution reaction 4-6, which takes place because of the pH diminution by water from coal and that were not present in the blank voltammograms because water concentration was not

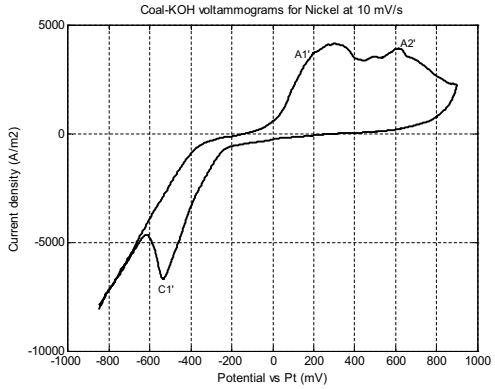

(a) Coal-KOH voltammogram on nickel at $10mV/s$

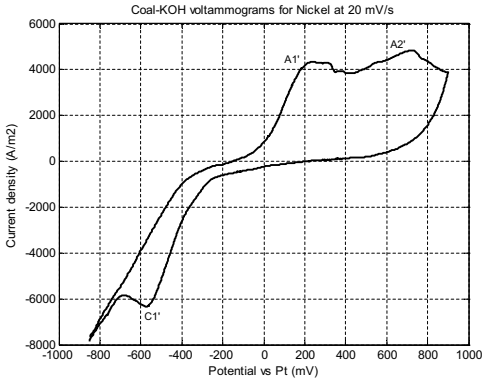

(b) Coal-KOH voltammogram on nickel at $20mV/s$

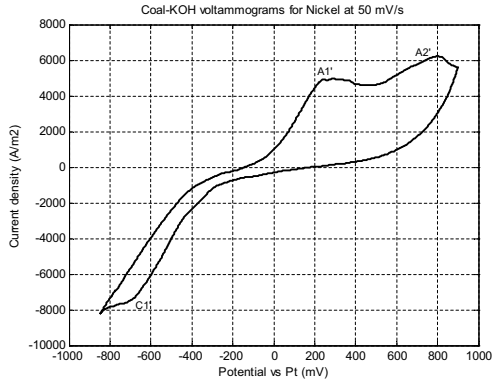

(c) Coal-KOH voltammogram on nickel at $50mV/s$

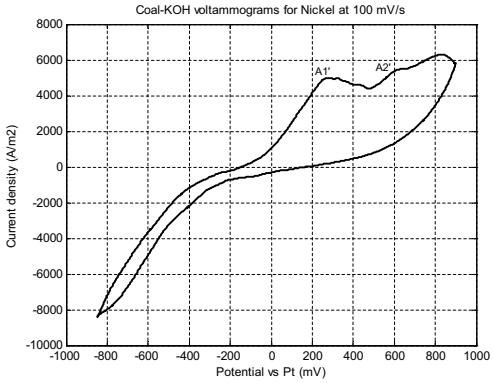

(d) Coal-KOH voltammogram on nickel at $100mV/s$

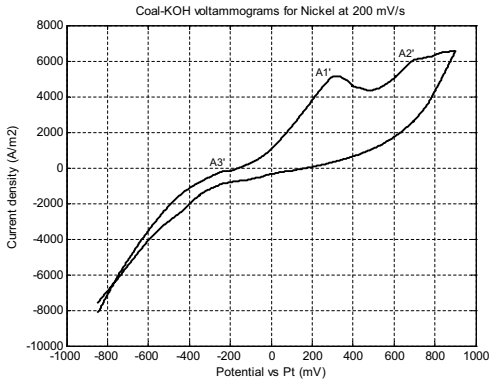

(e) Coal-KOH voltammogram on nickel at $200mV/s$

Figure **4-3**: Cyclic voltammograms for Coal-KOH mixture using Nickel as electrode

Table **4-4**: Tafel optimized parameters values

Tafel slope (mV/dec)	i_0 (A/m^2)	α	n	σ^2	R^2
218	83.7	0.47	1.37	$3.21 * 10^{-7}$	0.99

enough to produce hydrogen at the evaluated potentials.

$$H_2O + e^- \rightarrow \frac{1}{2}H_2 + OH^- \tag{4-6}$$

When subjecting the coal-KOH mixture to the potential sweep, a high and width oxidation peak, denoted as A1', and another not as high and with, A2', at higher potentials appear. These peaks should be related with the oxidation of materials from coal. The added materials are organic matter, moisture and ash, as tabulated in tables **4-1** and **4-2**. The composition of ash is mainly SiO_2 and Al_2O_3 accompanied by minor quantity of metallic oxides. So, ash composition should be very similar to that of the alumina tubes, see table **4-3**, and it could be said that ash is inert in the process of electrochemical oxidation. Water has the effect of reducing the pH of the liquid and its effect is clearly evidenced by the evolution of H_2. Because of the anterior arguments, it could be said that the currents that arise during the oxidation sweeps probably are related to organic matter oxidation.

At $200mV/s$ a third peak, A3', can be seen. This process could be related with reaction 4-6 . The reason to see this peak only at high sweep velocities is that it is a fast process.

Tafel behaviour was identified in the overpotential range from 200 mV to 250 mV. The graphs for the identified zone and the data fit are illustrated in figure **4-4**. The continuous line in figure 4.4(b) was obtained by minimization of quadratic error by comparing process data, circles, with the Tafel equation, equation 4-7. During the process of optimization, the Tafel parameters, n, α and i_0, were calculated by implementing the function fmincon in Matlab. The values of these parameters and of the variance and regression coefficient are tabulated in table **4-4**.

$$\eta = log(i)\frac{2.303RT}{nF(1-\alpha)} - log(i_0)\frac{2.303RT}{nF(1-\alpha)} \tag{4-7}$$

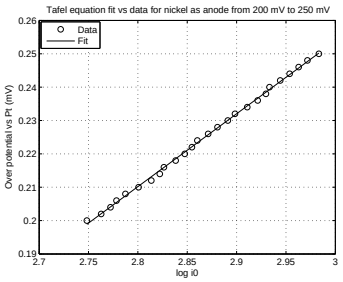

(a) Tafel fit of process A1' using nickel as electrode

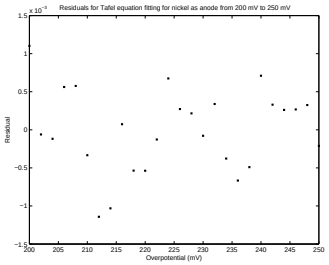

(b) Residuals for Tafel fit of process A1' using nickel as electrode

Figure **4-4**: Tafel plot analysis for the oxidation process A1' using nickel as electrode

The high value associated with i_0 in this case and the fact that the transfer coefficient, α, has also a high value indicates firstly that nickel could be suitable for the electrochemical oxidation of organic dissolved coal molecules in this molten KOH media and secondly that these reactions should be a complex set of charge transfers steps [22] which, according to the obtained voltammograms, are probably irreversible. Although, as said before, thousands of reactions could occur and their nature is probably very complex, the calculated value for n indicates that a one electron transfer step should be the rate determining step of this set of reactions. If the electro-active species are products of homogeneous chemical reactions with high equilibrium constants that precede probably irreversible charge transfer reactions, then homogeneous processes should not have any influence in the limiting process of charge transfer at the electrical double layer, as stated in [10]. However, a deep study for this complex system is necessary to corroborate these assumptions.

4.1.2 Iconel welding alloy

For the case of inconel welding alloy, blank voltammograms show a marked peak, A1, which is attributed to the mentioned reactions 4-1 and 4-2. This peak reduces, apparently, gradually in intensity with the increase of sweep velocity. However, this reduction in the high of the peak should be the effect of time. The first voltammogram was at $10mV/s$ and the last corresponded to $200mV/s$. So, at the first voltammogram the peak is higher than at the other velocities because the surface was clean and the major part of it is passivated. While time passes, the surface becomes more passivated until it reaches a total coverage by nickel oxidized species and because pH and potential of the system are not sufficiently low to recover metal nickel phase, this signal disappears with time.

For the case of the voltammograms for the coal-KOH mixture, it is seen a process, A1', which could be the same associated with organic reactions over nickel passivated surface as in the

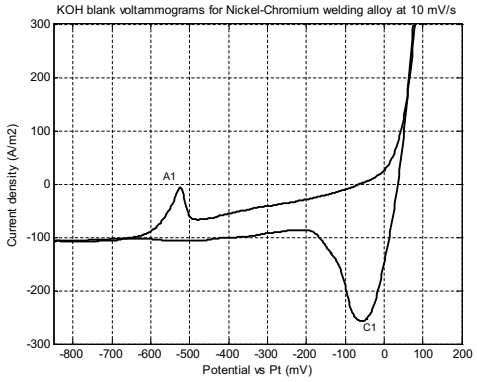

(a) KOH blank voltammogram on Inconel welding alloy at $10mV/s$

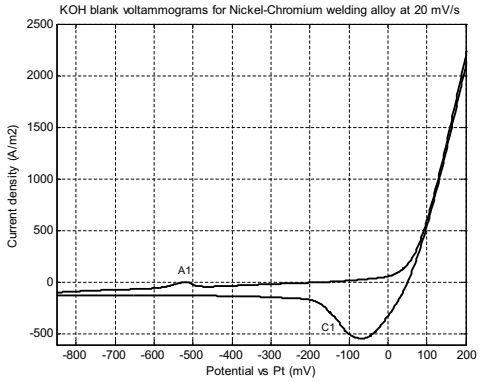

(b) KOH blank voltammogram on Inconel welding alloy at $20mV/s$

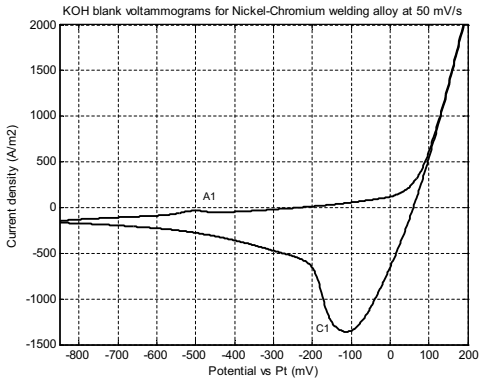

(c) KOH blank voltammogram on Inconel welding alloy at $50mV/s$

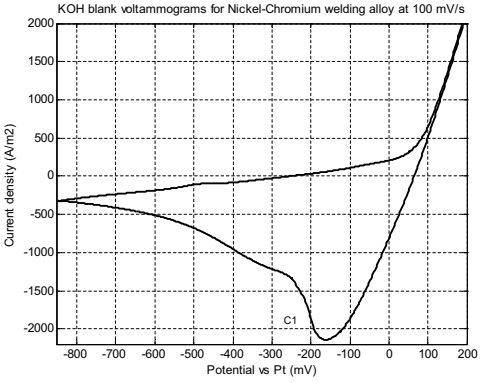

(d) KOH blank voltammogram on Inconel welding alloy at $100mV/s$

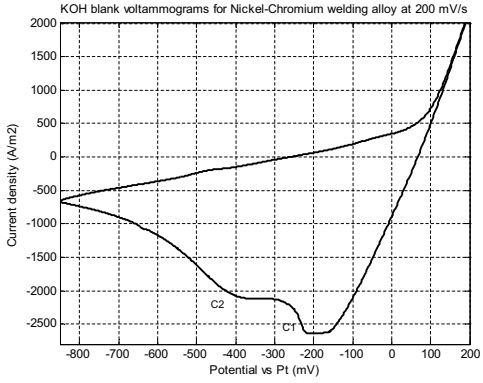

(e) KOH blank voltammogram on Inconel welding alloy at $200mV/s$

Figure **4-5**: Cyclic voltammograms for KOH using Inconel welding alloy as electrode

case for nickel wire. However, in contrast to the observed behaviour for this last material, voltammograms in figure **4-6** show that peak A1' decays near to zero current density after the maximum has been reached. This occurs because electroactive species are depleted, almost in the diffusion layer, and because at the corresponding potentials another species oxides, different to nickel oxide or hydroxide, are favoured. One reason to this affirmation is the presence of the second peak A2', after the non faradaic zone, that did not appeared in the case of nickel wire. This peak has been attributed to chromium oxides, as will be explained for the case of 410 stainless steel. So, when the electrode is composed by different materials, as is the case for inconel welding, different regions of potentials to generate charge transfer could be present whereas when the material is composed by similar materials these potentials for electron transfer remain similar and that is the reason because current density does not decays to a non faradaic zone when using nickel wire as electrode.

After the depletion of reactions over chromium oxides it is observed that at high sweep velocities a process A3', probably related with reaction 4-5, appears. This is in accordance with thermodynamics [5] and [30]. This peak is different to that named A2' in figure **4-3** which should be due to oxidation of organic species over passivated nickel phases.

Tafel behaviour was also evaluated for this material. The graph is illustrated in figure 4.9(a). The continuous line was obtained by minimization of quadratic error by comparing process data, circles, with the Tafel equation, equation 4-7. During the process of optimization, the Tafel parameters, n, α and i_0, were calculated by implementing the function fmincon in Matlab. The values of these parameters and of the variance and regression coefficient are tabulated in table **4-5**.

The extracted information above suggest firstly that near to 50% of the potential difference across the double layer is inverted to a one electron transfer process which is the controlling one.

Secondly, by observing the figure **4-6**, it can be seen that only at high potential sweep velocities the process A4' arises. This could be the same process A1 seen for the blank voltammograms. The reason to see this process at higher velocities in the presence of dissolved coal with respect to the blanks could be that in the absence of dissolved coal products, only molecules related with molten KOH adsorb on the metal surface, whereas in the presence of another species different adsorption processes slower than hydroxide ions adsorption take place.

The intensities of the second peak, A2', for the mixture have also been quantified and shown in table **4-6**. A characteristic of this process is that it increases in intensity as increasing the sweep velocity and at sufficient high velocities its height is greater than that of peak

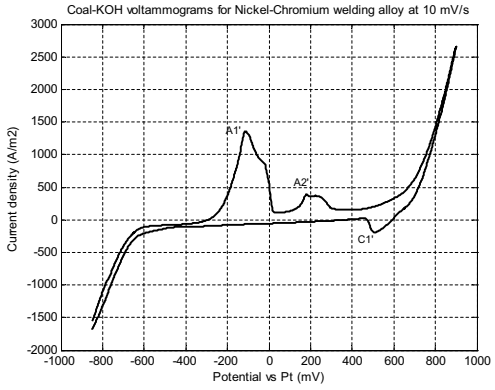

(a) Coal-KOH voltammogram on Inconel welding alloy at $10mV/s$

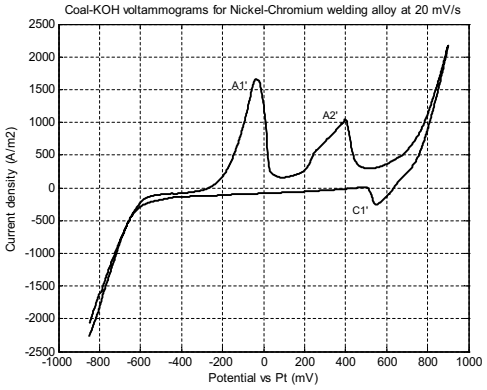

(b) Coal-KOH voltammogram on Inconel welding alloy at $20mV/s$

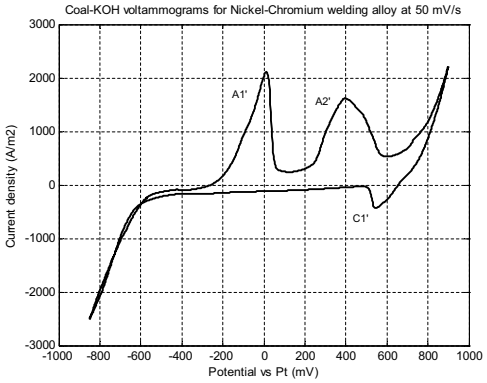

(c) Coal-KOH voltammogram on Inconel welding alloy at $50mV/s$

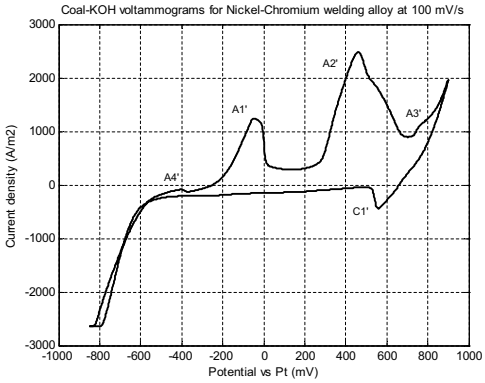

(d) Coal-KOH voltammogram on Inconel welding alloy at $100mV/s$

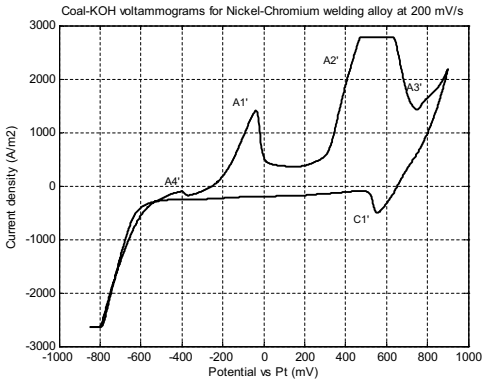

(e) Coal-KOH voltammogram on Inconel welding alloy at $200mV/s$

Figure **4-6**: Cyclic voltammograms for Coal-KOH using Inconel welding alloy as electrode

Table **4-5**: Tafel optimized parameters values estimated for Inconel welding alloy as electrode

Tafel slope (mV/dec)	i_0 (A/m^2)	α	n	σ^2	R^2
140.6	28	0.47	1.43	$6.05 * 10^{-7}$	0.99

A1'. At $200mV/s$ a zone of saturation in the signal for current density appears because the produced current overcomes equipment resolution.

The lower values of i_0 for this material, in contrast with those estimated for nickel wire, as can be seen in table **4-5**, indicate that the presence of new species different to nickel reduces the electro-catalytic activity of the material because of the reduction of the number of active sites for the reactions. Also, the value for the transfer coefficient, which is very different to that for nickel, suggests that oxidation processes have a different nature on this surface.

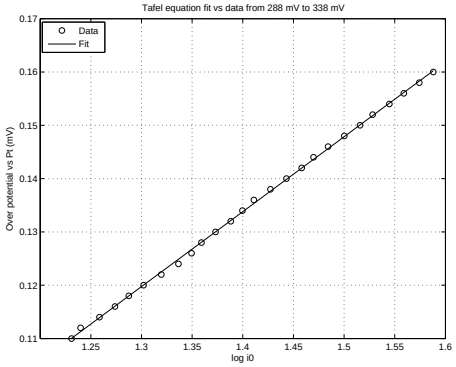

(a) Tafel fit for inconel welding alloy as electrode

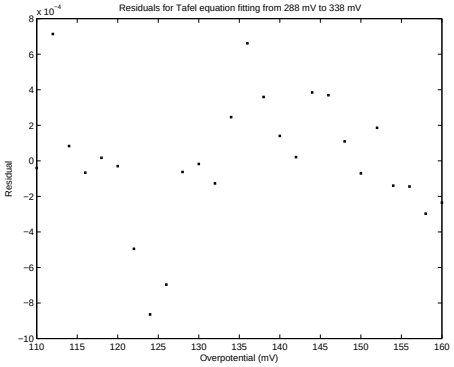

(b) Tafel plot of process A1' using inconel welding alloy as electrode

Figure **4-7**: Tafel plot analysis for the oxidation process A1 using inconel welding as electrode

A curious behaviour can be observed if inconel alloy welding is subjected to a new cyclic voltammetry program after being used before. Figure **4-8** shows the voltammograms for the coal-KOH mixtures using the welding as electrode, but this welding was subjected before to the experiments represented by figure **4-6**. In this new set of voltammograms it is observed that the intensity of the peak which corresponds to that assigned to reactions catalysed by chromium oxides reactions lowers. This could be explained by the possible precipitation of chromium carbides at temperatures at which carbides are unstable and chromium depleted zones are developed. This depletion of chromium which could be related with the cooling rate of the material after its usage in the preceding experiments [18] could be the fact that

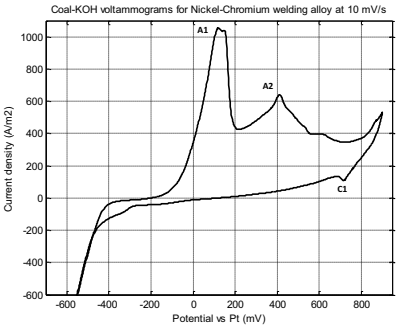

(a) Coal-KOH voltammogram on Inconel welding alloy at $10mV/s$

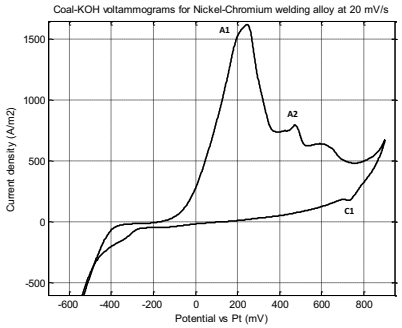

(b) Coal-KOH voltammogram on Inconel welding alloy at $20mV/s$

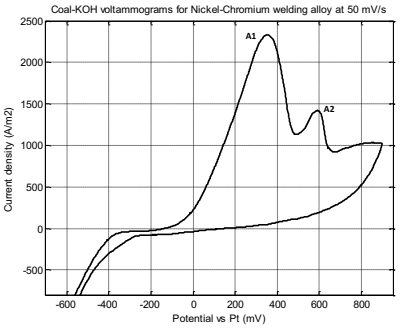

(c) Coal-KOH voltammogram on Inconel welding alloy at $50mV/s$

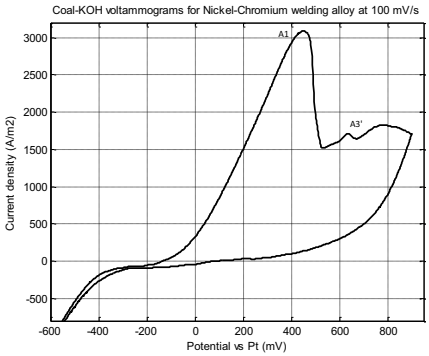

(d) Coal-KOH voltammogram on Inconel welding alloy at $100mV/s$

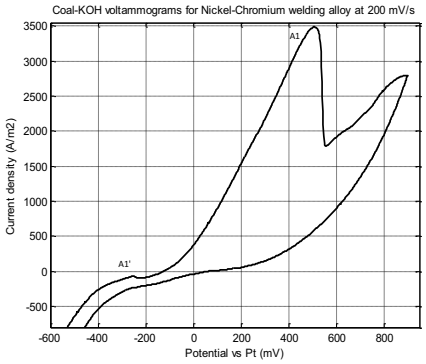

(e) Coal-KOH voltammogram on Inconel welding alloy at $200mV/s$

Figure **4-8**: Cyclic voltammograms for Coal-KOH using chromium deficient Inconel welding alloy as electrode

Table **4-6**: Inconel welding alloy second oxidation peak analysis for the coal-KOH mixture

v(mV/s)	E_p(mV/s)	$E_{p/2}$	$i_p(A/m^2)$
10	198	151	253
20	388	261	822
50	400	296	1351
100	458	349	2138

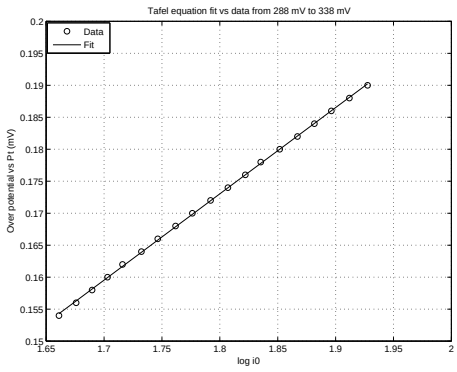

(a) Tafel fit of process A1 for the chromium deficient Inconel welding alloy

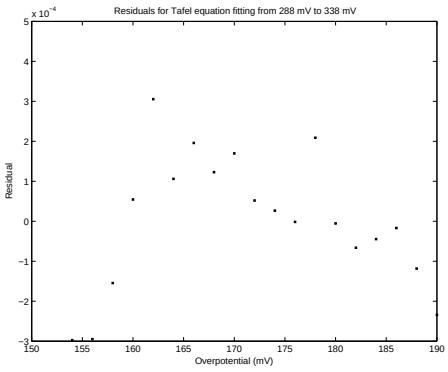

(b) Residuals for Tafel fit of inconel welding alloy as electrode

Figure **4-9**: Tafel plot analysis for the oxidation process A1 using inconel chromium deficient as electrode

Table **4-7**: Tafel optimized parameters values estimated for chromium deficient Inconel welding alloy as electrode

Tafel slope (mV/dec)	i_0 (A/m^2)	α	n	σ^2	R^2
134.8	32.8	0.46	1.39	$3.19 * 10^{-8}$	1.00

explains the reduction in the second peak intensity, as will be explained later for the case of 410 stainless steel.

The chemical composition of this alloy is shown in table **4-8**. Carbon and chromium elements are present in this alloy, which makes it possible the formation of chromium carbides when using this alloy.

Table **4-8**: Nickel-Chromium welding chemical composition

Element	Percentage
Ni	Balance
C	0.025
Mn	6.0
Fe	6.0
S	0.015
Si	0.4
Cu	<0.50
Ta	<0.08
Cr	16
Nb	2.2
Co	<0.08

The depletion of chromium does not affect the kinetics of the process and this is corroborated by the values of the exchange current densities and the transfer parameters calculated for the non sensitized and sensitized electrodes. The values of Tafel parameters and of the variance and regression coefficient are tabulated in table **4-7**. The formation of chromium depleted zones has not any appreciable influence on the organics electrooxidation.

4.1.3 410 Stainless steel

The voltammograms for this electrode are characterized by the presence of various easily visible processes, as shown in figures **4-10** and **4-11**. Also, a quantitative analysis for the oxidation peaks have been made to explore the catalytic activity to organic reactions of the electrode.

Focussing in the tables **4-9** and **4-10** it is seen that the first process of oxidation occurs at nearly the same potentials for the blank and the mixture coal-KOH, but the current density in presence of the dissolved coal is reduced. This phenomena could be related with a diffusional restriction which diminishes the approximation rate of electroactive species from the liquid. This process, A1, could be related with reaction 4-8.

$$Fe + 2OH^- \rightarrow Fe(OH)_2 + 2e^- \tag{4-8}$$

By the other hand for the process named A3', in the voltammograms for coal-KOH mixtures, it can be seen that the current density increases when dissolved coal is present. This is also related with the catalytic activity of metal oxides which could be chromium oxides rather than iron oxides because the peak A3' could not correspond to the restructuring of the anode surface layer because in this investigation it appeared at a position much far from peak A2'.

However, chromium species stability and stoichiometry has been found to be very complicated as reported elsewhere [22], [4]. A deeper study must be done to understand and try to elucidate what kind of processes are involved with chromium. During the experimentation, it was observed that a a black film appeared in both electrodes. This oxide film formed on the surfaces has been reported to have a higher degree of disorder than that that could be formed on pure nickel [27]. Also, it is believed that this film consists on a bi-layered structure with an outer hydroxide layer, $Cr(OH)_3$, and an inner oxide layer, Cr_2O_3, according to [4]. With respect to this fact it could be helpful to implement EIS analysis to the electrodes to confirm this hypothesis because the information with which it was developed considers chromium solutions at different pH values and temperatures and no molten hydroxide, as in the case of this work.

With the information obtained in the literature and in analogy with iron, here it is proposed the possible reactions concerning to chromium in the system studied, but as mentioned earlier, more studies and complementary techniques must be implemented to confirm the hypothesis.

$$Cr + 3OH^- \rightarrow Cr(OH)_3 + 3e^- \tag{4-9}$$

$$Cr(OH)_3 + OH^- \rightarrow 2H_2O + CrO_2^- \tag{4-10}$$

$$CrO_2^- + 4OH^- \rightarrow CrO_4^{2-} + 2H_2O + e^- \tag{4-11}$$

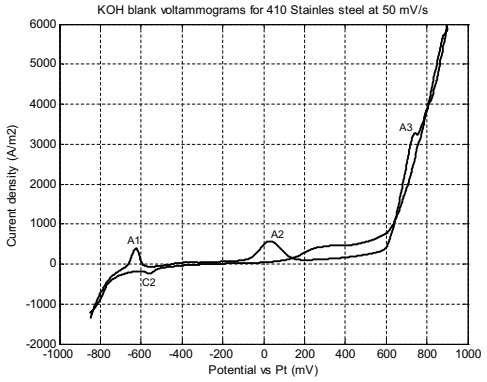

(a) KOH blank voltammogram on 410 Stainless Steel at $50mV/s$

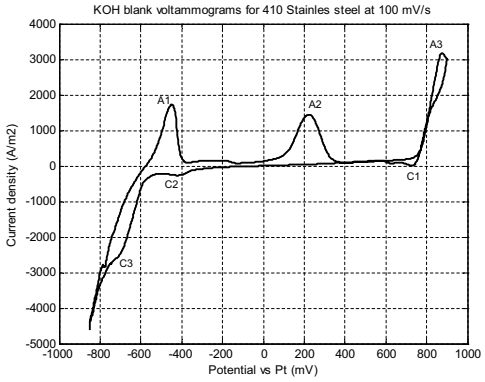

(b) KOH blank voltammogram on 410 Stainless Steel at $100mV/s$

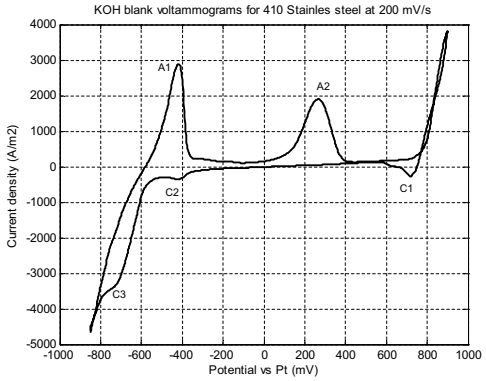

(c) KOH blank voltammogram on 410 Stainless Steel at $200mV/s$

Figure **4-10**: Cyclic voltammograms for KOH using 410 Stainless Steel as electrode

One important fact to highlight is the possibility to generate ionic species, products of reactions derived from electrochemical oxidation processes. From the process corresponding to peak A2, which could be attributed to reactions 4-12 or 4-13, iron oxides or hydroxides could react homogeneously to form the precursor species of the soluble ferrate ion and could be represented by reactions 4-14, 4-15 and 4-16.

$$Fe(OH)_2 + OH^- \rightarrow Fe(OH)_3 + e^- \tag{4-12}$$

$$2Fe(OH)_2 + 2OH^- \rightarrow Fe_2O_3 + 3H_2O + 2e^- \tag{4-13}$$

$$Fe(OH)_2 + 2OH^- \rightarrow FeO_2^{2-} + H_2O \tag{4-14}$$

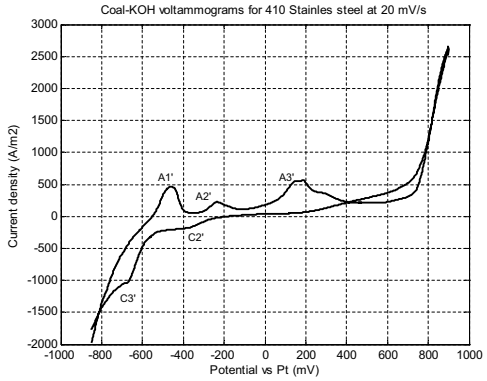

(a) Coal-KOH voltammogram on 410 Stainless Steel at $20mV/s$

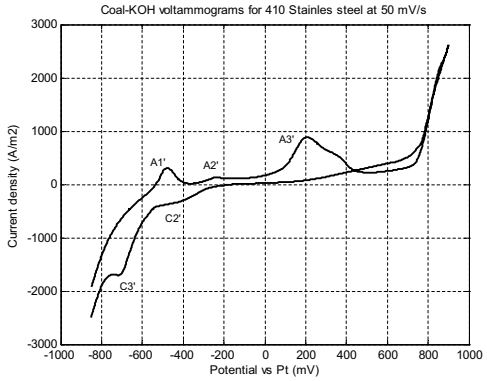

(b) Coal-KOH voltammogram on 410 Stainless Steel at $50mV/s$

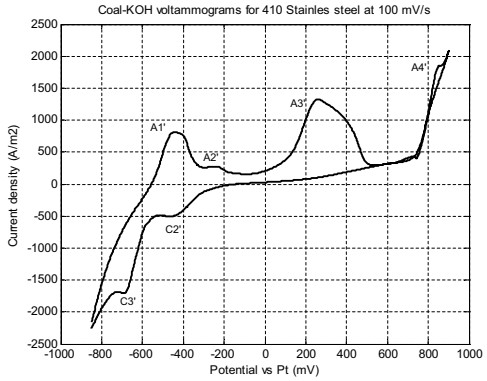

(c) Coal-KOHvoltammogram on 410 Stainless Steel at $100mV/s$

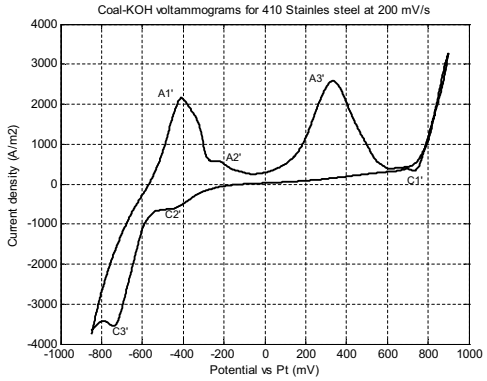

(d) Coal-KOH voltammogram on 410 Stainless Steel at $200mV/s$

Figure **4-11**: Cyclic voltammograms for Coal-KOH using 410 Stainless Steel as electrode

Table **4-9**: 410 stainless steel first oxidation peak analysis for the blank

v(mV/s)	E_p(mV/s)	$E_{p/2}$	$i_p(A/m^2)$
50	-574	-578	41
100	-458	-324	728
200	-424	-455	1324

Table **4-10**: 410 stainless steel first oxidation peak analysis for the coal-KOH mixture

v(mV/s)	E_p(mV/s)	$E_{p/2}$	$i_p(A/m^2)$
20	-484	-500	186
50	-492	-507	167
100	-464	-489	360
200	-418	-451	863

$$Fe(OH)_3 + OH^- \rightarrow FeO_2^{2-} + 2H_2O \tag{4-15}$$

$$Fe_2O_3 + 2OH^- \rightarrow 2FeO_2^{2-} + H_2O \tag{4-16}$$

Also a non-stoichiometric magnetite formation on the electrode surface could arise followed by subsequent heterogeneous steps to produce iron dioxide ion
.

$$Fe(OH)_2 + 2OH^- \rightarrow Fe_3O_4 + 4H_2O + 2e^- \tag{4-17}$$

$$2Fe_3O_4 + 2OH^- \rightarrow 3Fe_2O_3 + H_2O + 2e^- \tag{4-18}$$

$$Fe_3O_4 + 4OH^- \rightarrow 3FeO_2^{2-} + 2H_2O + e^- \tag{4-19}$$

Another posibility for the first oxidation process has been reported by [20] to be due to the heterogeneous reaction 4-20.

$$Fe + 4OH^- \rightarrow FeO_2^{2-} + 2H_2O + 2e^- \tag{4-20}$$

Then the iron dioxide ion reacts over the electrode surface to produce the ferrate (IV) species, reaction 4-22, in parallel with the iron oxyhydroxide formation, reaction 4-21, attributed to peaks A4 or A3', at the potentials corresponding to oxygen evolution reaction, analogous to the nickel case as stated in [30], [36]. So, if no oxygen is produced at the electrode these

processes can't occur because the overpotentials are very close to that required for reaction 4-23, proposed in [28].

$$Fe(OH)_2 + OH^- \rightarrow FeOOH + H_2O + e^- \tag{4-21}$$

$$FeO_2^{2-} + 4OH^- \rightarrow FeO_4^{2-} + 2H_2O + 3e^- \tag{4-22}$$

$$2OH^- \rightarrow \frac{1}{2}O_2 + H_2O + 2e^- \tag{4-23}$$

The ionic nature of the products of iron species oxidation suggest that the electrode dissolves at the conditions of operation making it an inappropriate material to be an anode for a dissolved coal products fuel cell in fused KOH.

As in the case for Inconel welding, this stainless steel also shows a sensitization behaviour. The same wire that was used for the mentioned results, was subjected to a new set of cyclic voltammetry experiments and in this second phase the metal dissolution was appreciable. This dissolution was not observed for the "new" material because the temperatures of the experiment were not sufficient high to carbon diffusion to the intergranular boundaries. But, after a high rate cooling process, as that implemented after the experiments, probably not sufficient austenite nucleation took place and this could provide the physical changes that enhanced the diffusion of carbon to the intergranular boundaries in the later experiments. This suggests that, probably, although the low temperature, $250^{\circ}C$, diffusive transport of carbon is sufficiently high to reach intergranular regions to produce chromium carbides and the respective chromium depleted zones that could be attacked by the media. In the figure **4-12** are shown the voltammograms for the blank and the mixture using this material as electrode. It can be observed that there is a point, named "X", at which the waves intercept and from this point the oxidative currents are below cathodic ones. The peak A2 in these voltammograms corresponds to an oxidation process over the renewed surface that arises because of the continuous metal dissolution and could correspond to the mentioned reactions 4-12 or 4-13.

4.1.4 Chromel alloy and Alumel alloys

Other two nickel alloys were evaluated, Chromel alloy composed by 90% of Ni and 10% of Cr and Alumel alloy composed by 95% of Ni, 2% Al, 2% Mn and 1% Si. This was done

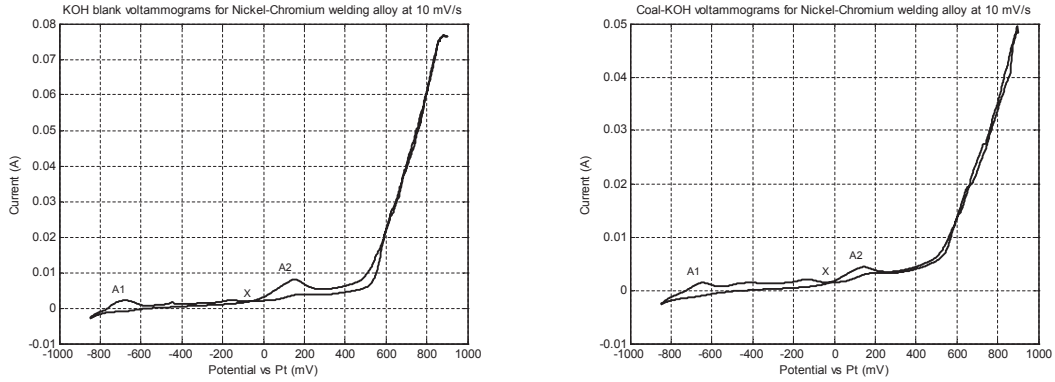

(a) KOH blank voltammogram for sensitized 410 Stainless Steel at $10mV/s$

(b) Coal-KOH voltammogram for sensitized 410 Stainless Steel at $10mV/s$

Figure **4-12**: Voltammograms for the sensitized 410 stainless steel at $10mV/s$

to corroborate the electrocatalytic activity of nickel to oxidizing organic materials from coal and to identify a global behaviour of nickel and its alloys in this process.

The respective blanks, figures **4-13** and **4-16**, show a very similar behaviour to that observed for nickel wire. However, some differences could be identified. First, for the case of chromel alloy, it can be seen that process C2, attributed to reaction 4-2, is closer to process C1, attributed to reaction 4-5, with respect to the case of nickel at low sweep velocities. At sweep rates greater than $50mV/s$ this behaviour is not longer observed. At $20mV/s$ is seen that peak C2 is not a single peak, but two peaks, C2 and C2', but this happened only for this voltammogram. One possible reason to explain why processes C1 and C2 are closer for the case of the chromel alloy is that reaction 4-5 is affected by chromium species in the solid phase in a way that more cathodic potentian is required to the reverse reaction to occur, that is, chromium species increases the irreversibility for this reaction. More rigorous work is needed to confirm this observation.

Another difference is the detection of the peak A1 in figures 4.16(a) and 4.16(b), for alumel case, which has been yet attributed to reaction 4-5, but that was not observed for the blanks at higher sweep rates. Also, in contrast to chromel alloy, peaks C1 and C2 seem to superpose at sweep rates below $200mV/s$ and appear at higher potentials. This means that aluminium species have a catalytic effect on the reverse parts of reactions 4-2 and 4-5 because a less cathodic potential is needed to the respective reductions at the same pH. However, also a more rigorous study is needed to corroborate this affirmation.

For the coal-KOH mixtures, both materials present a similar behaviour of peak separation which was not observed for nickel and Inconel welding. This separation is attributed to

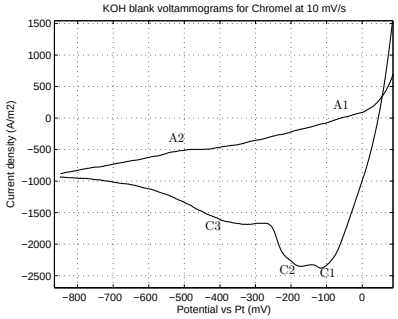

(a) KOH blank voltammogram on Chromel alloy at $10mV/s$

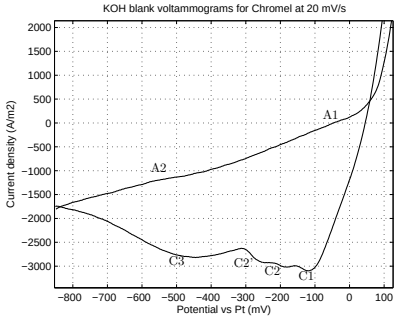

(b) KOH blank voltammogram on Chromel alloy at $20mV/s$

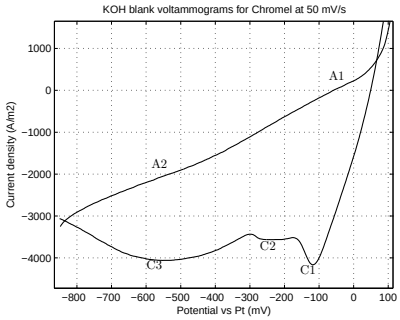

(c) KOH blank voltammogram on Chromel alloy at $50mV/s$

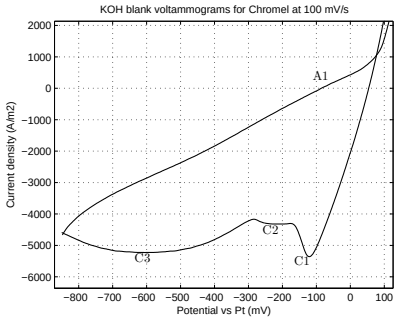

(d) KOH blank voltammogram on Chromel alloy at $100mV/s$

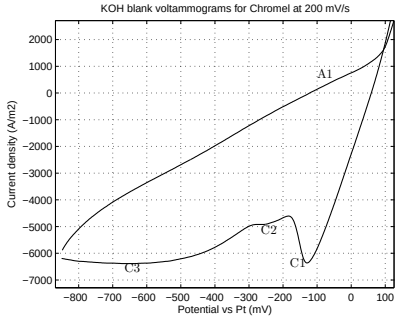

(e) KOH blank voltammogram on Chromel alloy at $200mV/s$

Figure **4-13**: Cyclic voltammograms for KOH using Chromel alloy as electrode

Table **4-11**: Tafel optimized parameters values for Chromel alloy as electrode

Tafel slope (mV/dec)	i_0 (A/m^2)	α	n	σ^2	R^2
126.5	26.6	0.44	1.42	$5.58 * 10^{-8}$	0.99

different reaction paths on the surfaces due to the possibly different crystallographic characteristics of the materials because of the possible distinct fabrication procedures for these materials which should involve differences in catalytic activity. The non faradaic zone present in the case of Alumel alloy is an indicative of this possible effect of fabrication procedure because, maybe, the nature of nickel oxidized species generated in this alloy is different to that of the nickel wire and that is because current density decays in the zone previous to oxygen evolution.

In the case of Chromel alloy it is seen that peak A2' increases with potential sweep velocity, as in the case of Inconel welding. Although peak separation is not as marked like in the case for Inconel welding, the global behaviour is maintained which could permit to conclude that chromium oxides are definitely active for organic species electrooxidation at potentials above that nickel oxides or hydroxides are active, peak A1'.

In table **4-11** it can be seen that, as in the case for the depleted chromium Inconel welding, electro kinetic behaviour changes. This Chromel wire was also used in a previous experiment, not shown here. So, the same reason of a possible sensitization of this material could be the cause to this behaviour, general for all nickel-chromium alloys. The Tafel plot for the calculations made by equation 4-7 are shown in figure **4-15**. In table **4-12** are tabulated the estimated Tafel parameters for Alumel alloy. The values for i_0 and α are greater than those for Chromel alloy which means that, although aluminium also has a detrimental effect in the catalytic activity for nickel, it is lesser than that of chromium. The Tafel plot for this alloy is shown in figure **4-18**.

Table **4-12**: Tafel optimized parameters values for alumel as electrode

Tafel slope (mV/dec)	i_0 (A/m^2)	α	n	σ^2	R^2
182.5	30.8	0.58	1.41	$1.37 * 10^{-7}$	0.99

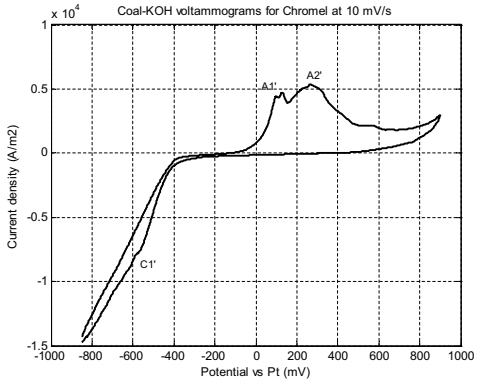

(a) Coal-KOH voltammogram on Chromel alloy at $10mV/s$

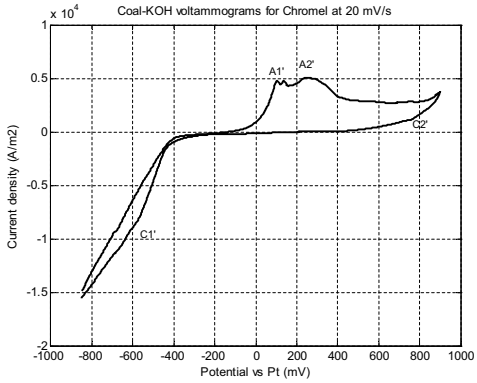

(b) Coal-KOH voltammogram on Chromel alloy at $20mV/s$

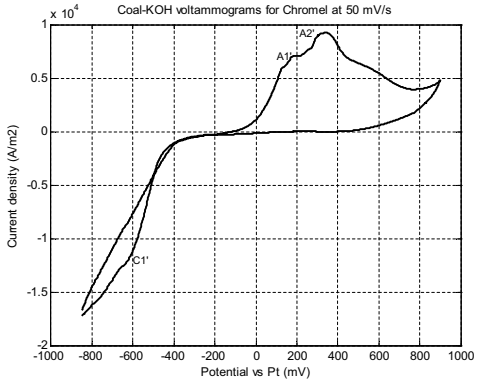

(c) Coal-KOH voltammogram on Chromel alloy at $50mV/s$

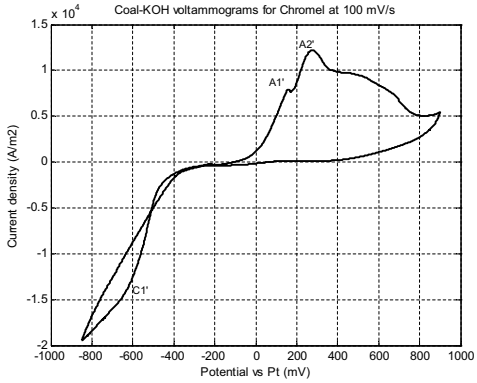

(d) Coal-KOH voltammogram on Chromel alloy at $100mV/s$

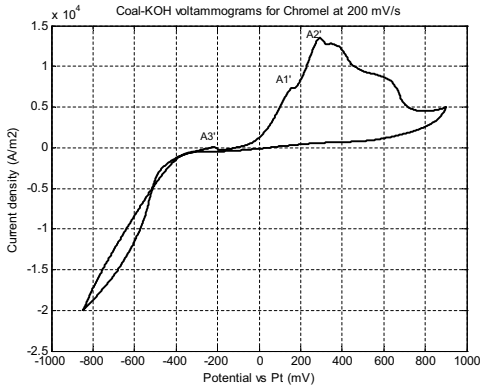

(e) Coal-KOH voltammogram on Chromel alloy at $200mV/s$

Figure **4-14**: Cyclic voltammograms for Coal-KOH using Chromel alloy as electrode

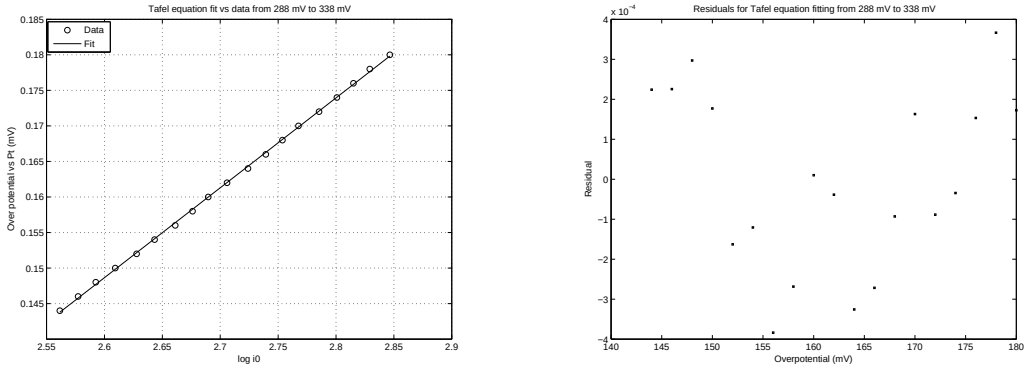

(a) Tafel fit of process A1' for Chromel alloy as electrode

(b) Residuals for Tafel fit of process A1' using Chromel alloy as electrode

Figure **4-15**: Tafel plot analysis for the oxidation process A1' using Chromel alloy as electrode

With the aim to increase the knowledge about the electro-catalytic behaviour of these alloys, a deeper analysis of materials could serve to explain the atomic reasons associated with the changes associated with reactivity and the differences in reactivity when nickel is alloyed with chromium or aluminium, but it is far from the objectives of this work.

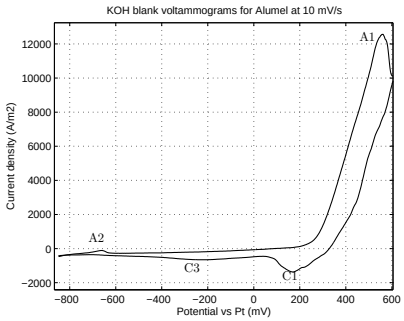

(a) KOH blank voltammogram on Alumel alloy at $10mV/s$

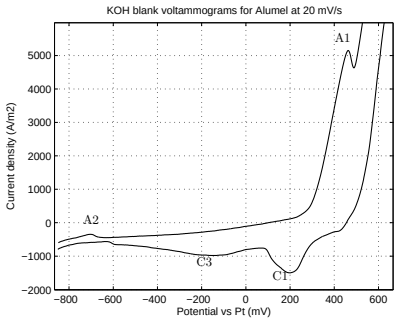

(b) KOH blank voltammogram on Alumel alloy at $20mV/s$

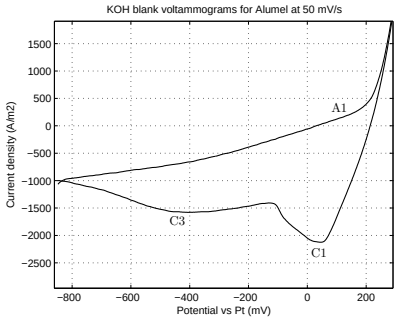

(c) KOH blank voltammogram on Alumel alloy at $50mV/s$

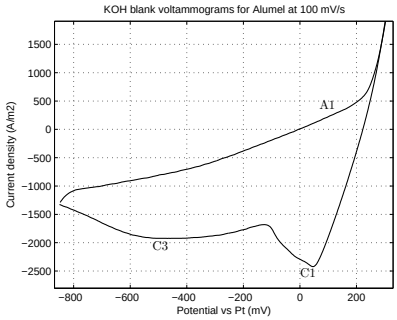

(d) KOH blank voltammogram on Alumel alloy at $100mV/s$

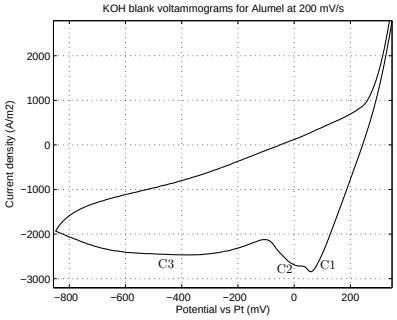

(e) KOH blank voltammogram on Alumel alloy at $200mV/s$

Figure **4-16**: Cyclic voltammograms for KOH using Alumel alloy as electrode

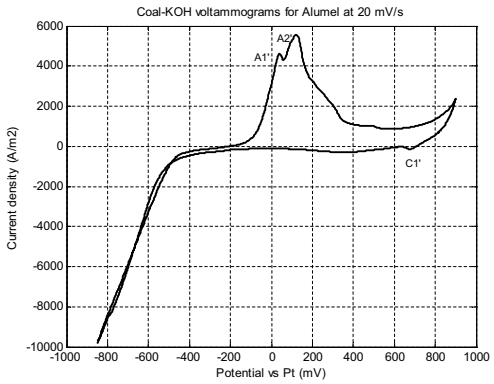

(a) Coal-KOH voltammogram on Alumel alloy at $20mV/s$

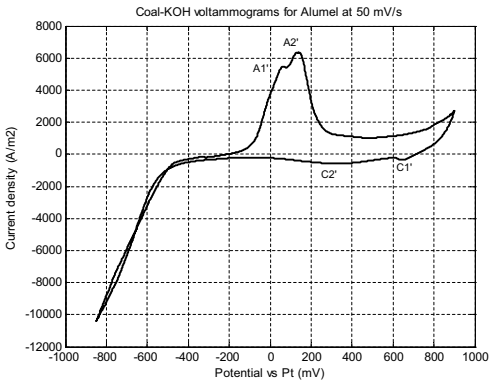

(b) Coal-KOH voltammogram on Alumel alloy at $50mV/s$

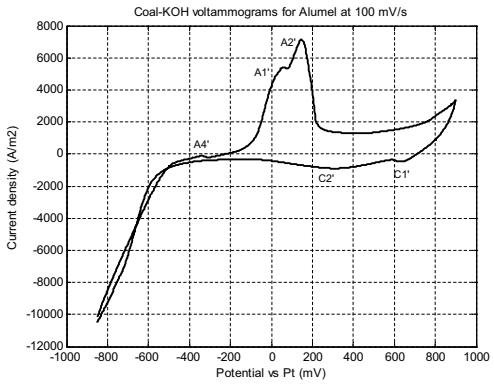

(c) Coal-KOH voltammogram on Alumel alloy at $100mV/s$

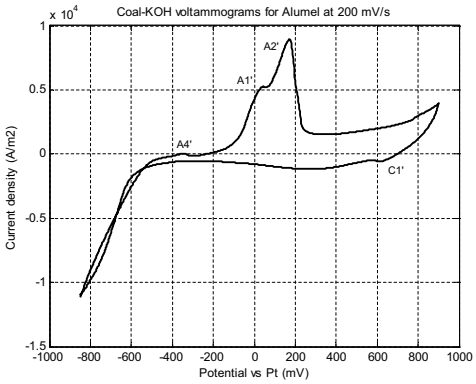

(d) Coal-KOH voltammogram on Alumel alloy at $200mV/s$

Figure **4-17**: Cyclic voltammograms for Coal-KOH using Alumel alloy as electrode

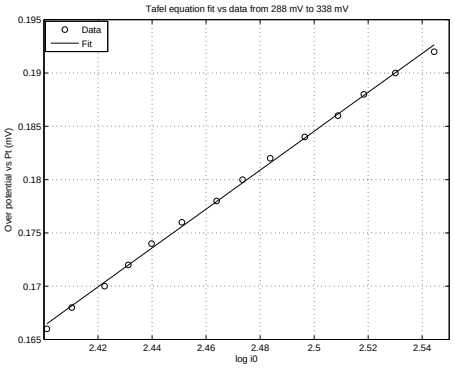

(a) Tafel fit of process A1' for alumel as electrode

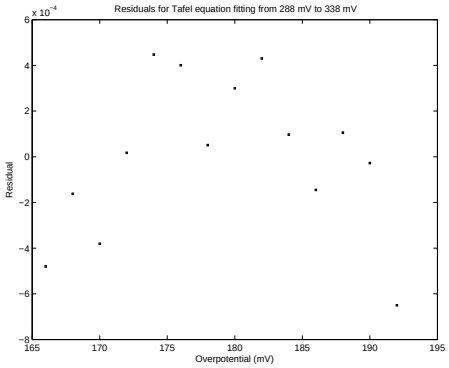

(b) Residuals for Tafel fit of process A1' using Alumel alloy as electrode

Figure **4-18**: Tafel plot analysis for the oxidation process A1' using Alumel alloy as electrode

5 Fuel cell model

5.1 Previous considerations and suppositions

- Electrochemical reactions at the porous electrodes are described by Butler-Volmer equation.

- The electroactive species concentration has been considered as very low compared with their respective solvents. Concentration of organics at the anode inlet has been estimated around 0.775 M according to calculations made by the equations reported for irreversible charge transfer processes [27].

- Electroactive species at the electrodes have been considered to be neutral molecules and the electrostatic potential is not considered in the species transport equations.

- The boundary condition at the exterior side of the anode considers that solid potential is zero while solid exterior side of the cathode is at the potential of the cell at a given polarization state. The other walls of the cell have been considered to be insulated.

- For liquid phase potential, it has been considered that walls different to walls of the electrodes are insulated.

- Fluids in both compartments have been considered to be incompressible.

To define the reactor geometry it was assumed that the process takes place in an ideally plug flow reactor with a ratio between concentration at outlet and inlet close to 0.55 and that mean fluid velocity is around $1mm/s$. Then a critic Reynolds was calculated using equation 5-1. [1].

[1] F. Coeuret. Introducción a la Ingeniería Electroquímica. 1992. Barcelona. Editorial Reverté. Capítulo 5. pp. 121

$$Re_{cr} = \frac{5.29 * 10^3}{(Sc^{\frac{2}{3}}(-ln\frac{C_o}{C_{in}}))^{0.8}} \tag{5-1}$$

Once the critic Reynolds was calculated, the real Reynolds for the process was calculated. This value should be lesser than the critic one and was calculated by the use of equation 5-2.

$$Re = 2\frac{uh}{\nu} \tag{5-2}$$

According to Coeuret, h should be at least 2 mm. The chosen value for h was 10 mm because at lesser values the simulation had convergence problems related with fluid flow at the anodic channel.

Once the Reynolds value was calculated, it was possible to define a mass transfer coefficient value by knowing that this model represents an anode composed by a group of metallic cloths. The equation 5-3 was used to this calculation because the calculated Reynodls lies between 4 and 150.[2].

$$k_m = 0.4(\frac{ud}{\nu})^{0.507} \tag{5-3}$$

With these values the reactor length was calculated by equation 5-4.

$$L = -\frac{uh}{k_m} ln\frac{C_o}{C_{in}} \tag{5-4}$$

The reactor width was selected to treat a volumetric flow around to $3.45 * 10^{-6}\ m^3/s$.

The table **5-1** shows the values for the previous calculations.

Although the calculated value of L was close to $1m$, it was necessary to reduce this value because of computer memory limitations. The chosen value was $0.54m$.

The figure 5.1 shows a general scheme of the simulated fuel cell. In this plane both, anode and cathode compartments are showed in conjunction with a $1mm$ membrane separator which was assumed to be electrically conductive.

The model has been solved using Comsol multiphysics software.

[2]Ibid. Capítulo 8. pp. 197

Table **5-1**: Previous design values

Parameter	value
Re_c	90.3
Re	7.44
k_m	$4.56 * 10^{-6}[m/s]$
L	$1[m]$
l	$0.44[m]$
h	$1 * 10^{-2}[m]$

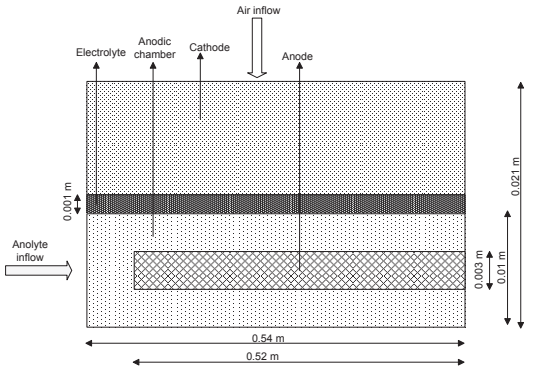

Figure **5-1**: General plane of the simulated fuel cell

5.2 Model equations and parameters

5.2.1 Current distribution

To calculate the cell current distribution the "Secondary Current Distribution" module has been used coupled with the "Diluted Species Transport" module for both, cathode and anode sides. The equations are shown below.

Current density in electrolyte phases for anode and cathode is represented by Ohm's law as stated in equations 5-5 and 5-6 with the respective correction due to electrode porosity, if necessary.

$$i_{la} = -k_{la}\epsilon_{la}^{1.5}\nabla\phi_{la} \tag{5-5}$$

$$i_{lc} = -k_{lc}\epsilon_{lc}^{1.5}\nabla\phi_{lc} \tag{5-6}$$

The divergence of the current density field for the electrolyte on each porous electrode is represented in equations 5-7 and 5-8 and it gives the relation for calculating the electrode potential distribution by a Poisson type equation.

$$\nabla \cdot i_{la} = i_{va} \tag{5-7}$$

$$\nabla \cdot i_{lc} = i_{vc} \tag{5-8}$$

The right side of equations 5-7 and 5-8 represents the volumetric current produced by the electrochemical reactions which can be calculated as the product of the local current density and the superficial active area per volume of electrode as showed in equations 5-9 and 5-10.

$$i_{va} = a_{ea} i_{loca} \tag{5-9}$$

$$i_{vc} = a_{ea} i_{locc} \tag{5-10}$$

The local current densities are functions of the electrode and electrolyte potentials at the electrolyte-electrode interface in the porous electrodes. These quantities could be represented by the well known Butler-Volmer equation as stated below by equations 5-11 and 5-12.

$$i_{loca} = i_{0a}(\exp(\frac{(1-\alpha_a)n_aF(\phi_{sa}-\phi_{la}-Eq_a)}{RT}) - \exp(\frac{-\alpha_a n_a F(\phi_{sa}-\phi_{la}-Eq_a)}{RT})) \tag{5-11}$$

$$i_{locc} = i_{0c}(\exp(\frac{\alpha_c n_c F(\phi_{sc}-\phi_{lc}-Eq_c)}{RT}) - \exp(\frac{-(1-\alpha_c)n_cF(\phi_{sc}-\phi_{lc}-Eq_c)}{RT})) \tag{5-12}$$

Analogously electrode phase potential is given by equations 5-13 and 5-14.

$$i_{sa} = -k_{sa}\epsilon_{sa}^{1.5}\nabla\phi_{sa} \tag{5-13}$$

$$i_{sc} = -k_{sc}\epsilon_{sc}^{1.5}\nabla\phi_{sc} \tag{5-14}$$

$$\nabla \cdot i_{sa} = -i_{va} \tag{5-15}$$

$$\nabla \cdot i_{sc} = -i_{vc} \tag{5-16}$$

To solve the potential distribution at the cell, the boundary condition at the exterior side of the anode considers that solid potential is zero, equation 5-17 while solid exterior side of the cathode is at the potential of the cell at a given polarization state, equations 5-18 and 5-19. The other walls of the cell were considered to be insulated, equation 5-20.

$$\phi_{sa} = 0 \tag{5-17}$$

$$\phi_{sc} = E_{cell} \tag{5-18}$$

$$E_{cell} = OCV - \phi_{sa} - V_{pol} \tag{5-19}$$

In which V_{pol} is varied between zero and 1.22 V, depending on the electrode material.

$$n \cdot \nabla\phi_{sf} = 0 \tag{5-20}$$

Analogously, for liquid phase potential it has been considered that walls are insulated in all parts for cathode and anode, equation 5-21.

$$n \cdot \nabla\phi_{lf} = 0 \tag{5-21}$$

By knowing the values of total current flowing through electrolyte and electrodes and the value of E_{cell} at a given polarization state in conjunction with the calculated reaction enthalpy it is possible to estimate the generated heat in the fuel cell, equation 5-22.

$$Q_{gen} = -I_T \frac{\Delta H_r}{n_e F} - I_T E_{cell} \tag{5-22}$$

5.2.2 Species transport

To determine the species concentration distribution at anode and cathode the following equations were solved.

$$\nabla \cdot (-D_i \nabla C_i + u_m \cdot C_i) = R_i \tag{5-23}$$

The boundary conditions to solve the concentration field are 5-24 and 5-25 at the inlet and outlet of each compartment. Equation 5-25 implies that there is no flux due to diffusion transport in the normal direction of flow at the outlet because there is no reaction at this region.

$$C_i = C_{in} \tag{5-24}$$

$$-n \cdot D_i \nabla C_i = 0 \tag{5-25}$$

The term at the right of equation 5-23 represents the reaction per unit volume and time and it is given by equations 5-9 or 5-10 depending on the electrode nature.

The diffusivity values for species at cathode were calculated by Maxwell-Stefan equation whereas at anode, the species diffusion was calculated from experimental voltammetry data using the equations reported by [10] and the calculated value was $4.72 * 10^{-6} cm^2/s$. This value is one order of magnitude lesser than the common one found for diffusion in liquid media, but this suggests that electroactive species are probably organic species of several hundred molecular weight.

5.2.3 Velocity field

The velocity field, u, is different in both compartments. The fluid flow at anode has been chosen to be due to forced convection while that at the cathode has been chosen to be due to transport of air merely by diffusion through the porous cathode. "Free and porous media" module was used to calculate the velocity field at the anodic chamber and "Darcy's law" module was used to calculate the respective velocity field at cathodic side. The equations are presented below.

Velocity field at anode side

Because there is a space in the anodic chamber that is not occupied by the porous electrode, at these regions the Navier-Stokes equation can be solved in a common way, equation 5-26 represents the equation for the velocity field in this case.

$$\rho_l(u_a \cdot \nabla)u_a = \nabla \cdot (-p_a I + \mu_l(\nabla u_a + (\nabla u_a)^T)) \tag{5-26}$$

Because fluid at anode side is liquid, it is considered to be incompressible and equation is valid.

$$\rho_l \nabla \cdot u_a = 0 \tag{5-27}$$

At the space occupied by the porous electrode matrix the Navier-Stokes equation must be modified to take into account the inherent properties of the porous material. Then equation 5-28 was applied.

$$\frac{\rho_l}{\epsilon_{sa}}((u_a \cdot \nabla)\frac{u_a}{\epsilon_{sa}}) = \nabla \cdot (-p_a I + \frac{\mu_l}{\epsilon_{sa}}(\nabla u_a + (\nabla u_a)^T) - \frac{2}{3\epsilon_{sa}}\mu_l(\nabla \cdot u_a)I) - \frac{\mu_l}{\kappa_a}u_a \tag{5-28}$$

Velocity field at cathode side

Velocity at this side of the cell was calculated by Darcy's law, equation 5-29 coupled with equation 5-30.

$$u_c = -\frac{\kappa_c}{\mu_{air}}\nabla p_c \tag{5-29}$$

$$\rho_{rho} \nabla \cdot u_c = 0 \tag{5-30}$$

The boundary condition for velocity at cathode is that the air inlet velocity is a function of pressure difference between ambient and porous media. This is shown in equation 5-31.

$$u_{inc} = -\frac{\kappa_c}{\mu_{air}} P - p_c \tag{5-31}$$

In table **5-2** are shown the parameter values used for the simulation.

5.3 Results

Simulations of fuel cells with different anode materials were performed in Comsol Multiphysics software. The results of these simulations are shown in this section.

Figure 5.3 shows the possible cell power with different anode materials. It is clear that nickel anode hast the best behaviour. The cell power has a magnitude lower than that reported by [9], but it is important to highlight that in the process simulated here the temperature is much lower than that needed for carbonate based fuel cells. Also, the difficulty of coal feed has been avoided because of coal dissolution in the molten hydroxide and that is the reason because the simulation has been performed by assuming continuous steady state conditions. Organic material has a very low concentration compared with that of KOH and the knowledge of the kinetic data permits to calculate the reaction path through the reactor. This implies that a molten hydroxide fuel cell offers important advantages that could be evaluated in a real experimental process with an stack of cells similar to the unit cell simulated here.

Table **5-3** shows the maximum obtainable power densities by implementing the different anode materials.

The figure 5.3 shows the polarization curves for the different fuel cells. These curves predict that the current-voltage relationship of these kind systems could be mainly represented by a primary current distribution because there is a long zone at which these relation seems to be linear, this behaviour has been reported by experimental work in [44].

Although, it is possible to identify charge transfer control zone for fuel cells using nickel, alumel and sensitized inconel electrodes. The extension of that regions ranges between 60

Table **5-2**: Simulation parameters

Parameter	value
T	$523[K]$
P	$1[atm]$
ϵ_{sc}	0.3
ϵ_{sa}	0.5
ae_a	$3500[1/m]$
ae_c	$3500[1/m]$
n_a	1
E_{qa}	$0.41[V]$
E_{qc}	$0.25[V]$
u_{in}	$0.001[m/s]$
ΔH_{rxn}	$448[kJ/mol]$
n_e	6
k_{la}	$164[S/m]$
k_{lc}	$1.12[S/m]$
μ_{air}	$2.78e-5[PaS]$
μ_l	$3.77e-3[PaS]$
ρ_{air}	$0.67[kg/m^3]$
ρ_l	$1790[kg/m^3]$
κ_a	$1e-5[m^2]$
κ_c	$1e-12[m^2]$

Table **5-3**: Maximum cell power density for different anode materials

Maximum cell power density (W/m^2)	Voltage (V)	Current density (A/m^2)	Material
160	0.35	476	Nickel
58	0.33	176	Alumel
59	0.33	175	Inconel welding

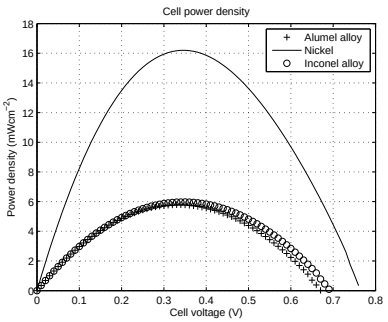

Figure **5-2**: Cell power comparison for the different simulated fuel cells

Table **5-4**: Predicted OCV for different anode materials

Voltage (V)	Material
0.76	Nickel
0.69	Inconel welding
0.67	Alumel

mV and 220 mV which is short compared to ohmic control zone, indicating that charge transfer processes are lower than ohmic processes only in a little fraction of voltage. For inconel welding and sensitized chromel electrodes, it is difficult to identify the charge transfer control zone.

The model also predicts that mass transfer control zone comprises a little fragment of the polarization curve for each fuel cell. The shortness of this region is an indicative that diffusion of the species is also a faster process compared to migration process in for a great voltage range.

The simulation also shows the possible OCV for the different fuel cells. OCV values close to those found in the literature [3], [9] and [24], over 1 V, were predicted only for fuel cell using nickel as anode, but the prediction for OCV in the range between 0.7 V and 0.8 V could be typical for processes with molten KOH as electrolyte according to data reported by [45] and values in this range were predicted for fuel cells using alumel and sensitized inconel anodes. Fuel cells with sensitized chromel and unused inconel welding present the lowest OCVs. In table **5-4** are shown the respective OCVs for each fuel cell.

The figures 5.3 shows the organics concentration distribution in the anode side at their respective maximum cell voltages.

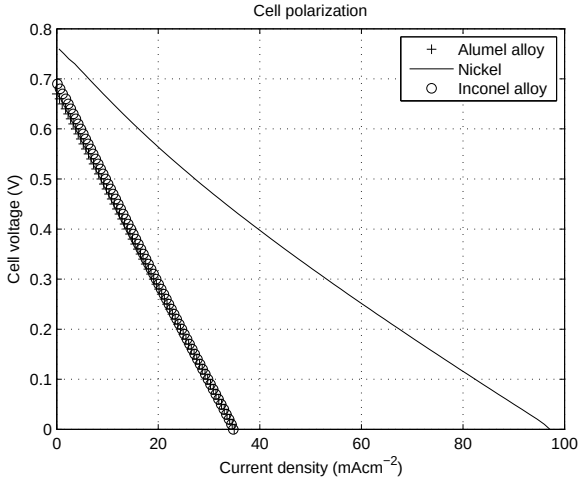

Figure **5-3**: Cell polarization comparison for the different simulated fuel cells

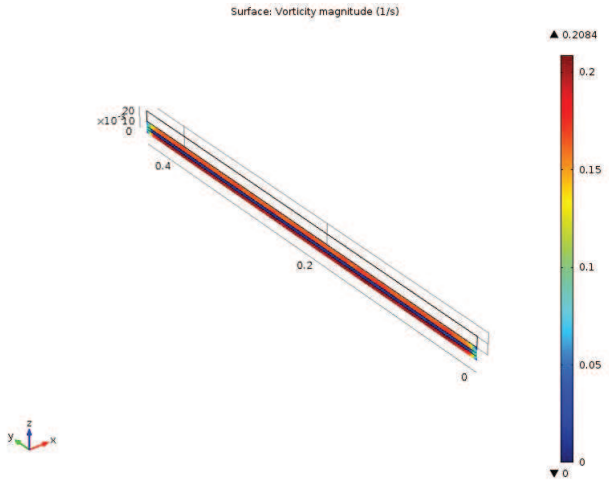

Figure **5-4**: Vorticity magnitude

The pressure distribution through the anodic channel is shown in 5.3. The magnitude of the pressure drop does not overcome 0.25 Pa which is favourable from the point of view that relative low power pumps could be adequate for the process.

FigureS **5-7** and **5-8** show the slices in yz planes for the potential distribution of electrolyte in the anode and cathode compartments. The potential distribution is appreciable in the flow direction of liquid KOH-coal mixture and is related with the change in concentration of electroactive species. In the anode compartment no distribution is appreciable. This is because it was proposed that air flows through anode in a perpendicular direction to xy plane and is always at the same concentration in the xz plane.

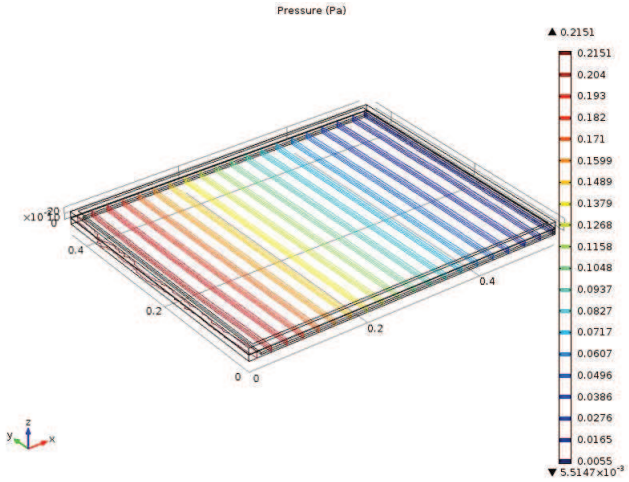

Figure **5-5**: Pressure drop through the anodic channel

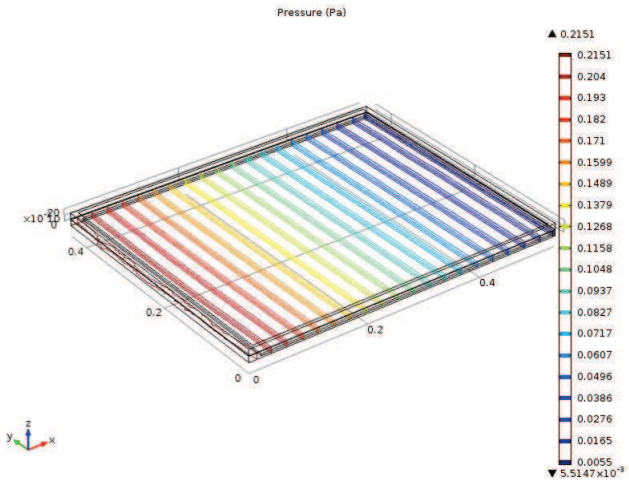

Figure **5-6**: Pressure drop through the anodic channel

The simulations show that it is possible to obtain electrical energy from electrochemical oxidation of organic species from coal dissolved in molten KOH and that high conversions could be obtained in a single device by using commercial nickel based materials as electrocatalyts. One part of the supplied energy could be compensated by the heat generated by current flow within the cell. Pressure drop across the electrodes is low and temperatures are not as high to require special materials for the construction of electrodes and cell body.

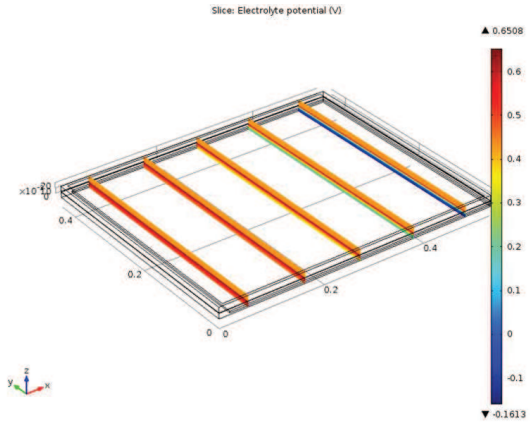

(a) Electrolyte potential distribution at highest cell voltage using nickel as anode

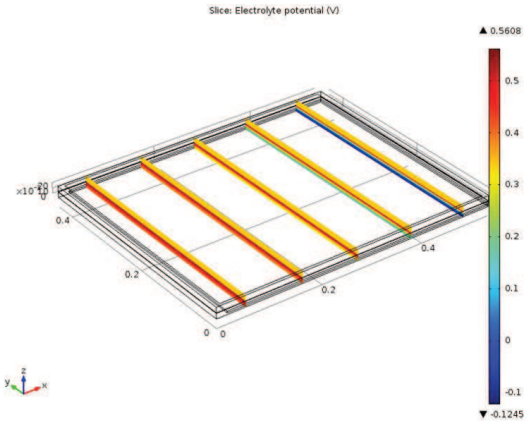

(b) Electrolyte potential distribution at highest cell voltage using alumel as anode

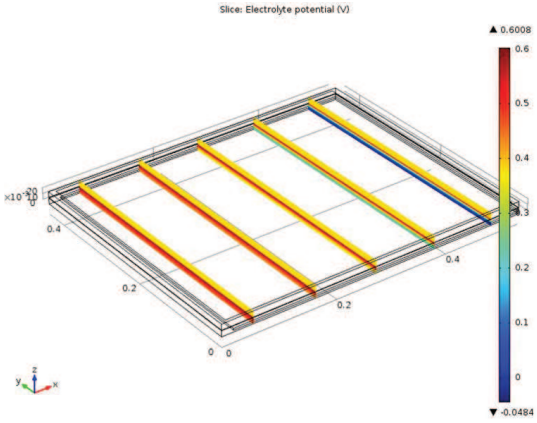

(c) Electrolyte potential distribution at highest cell voltage using sensitized inconel welding as anode

Figure **5-7**: Electrolyte potential distribution using nickel, alumel and sensitized inconel welding as electrodes

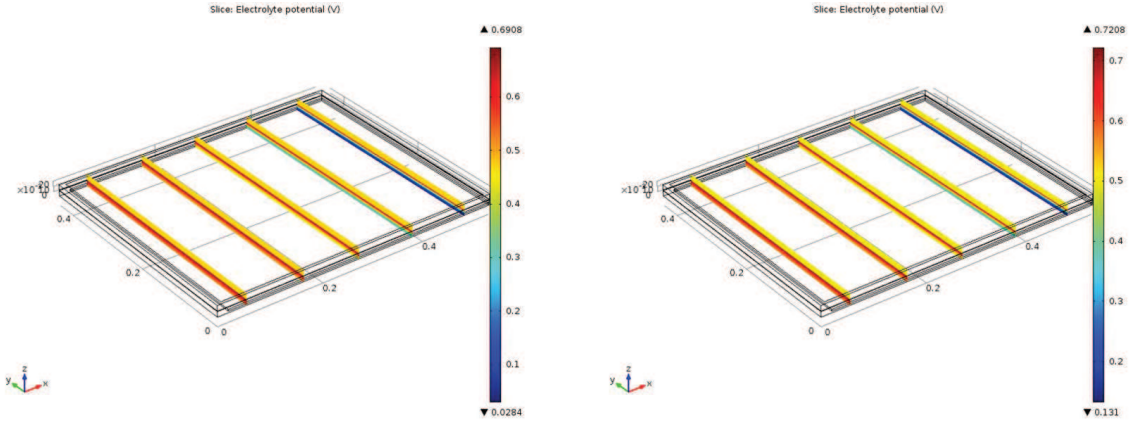

(a) Electrolyte potential distribution at highest cell voltage using sensitized chromel as anode

(b) Electrolyte potential distribution at highest cell voltage using inconel welding as anode

Figure **5-8**: Electrolyte potential distribution using sensitized chromel and unused inconel welding as electrodes

6 Conclusions and recommendations

6.1 Conclusions

The electrocatalytic behaviour of nickel, nickel-aluminium and nickel-chromium alloys has been evaluated by cyclic voltammetry. The voltammograms indicate that it is possible to oxidise dissolved organic compounds from coal in molten KOH at 250 ^{0}C on passivated surfaces which nature could be $NiOH_2$, NiO_2 or $NiOOH$. The calculated values for the exchange current densities of the different anodes, estimated for the possible first observable oxidation process, suggest that the electrocatalytic activity of nickel is greater than that of its aluminium and chromium alloys, at least, in the overpotential region evaluated for Tafel behaviour. The presence of these kind of metals affect the kinetic behaviour of nickel oxides reducing their electrocatalic activity towards organic molecules. These results have been used for solving part of a proposed model for a DCFC in molten KOH for the oxidation of dissolved coal compounds in this media at 250 ^{0}C.

The results of the simulation indicate that ohmic losses are the main overpotential contributors, especially losses at the solid electrolyte separator, and that the maximum obtainable power density, with dissolved sibbituminous coal in molten KOH and with a porous nickel electrode as anode, is of the same order of some reported experimental results which have been obtained at temperatures much higher than 250 ^{0}C and by using fuels like graphite, activated carbon and acid pretreated bituminous coal.

In this study it has been demonstrated, theoretically, that it is possible to use a globally available fuel, with no pretreatments, in a DCFC at relative low temperatures for obtaining electric energy .

6.2 Recommendations

It is of major importance the construction of a prototype fuel cell to confirm the simulation results and to evaluate the behaviour of the construction and electrode materials in a long time period because it is intended to develop a technology which be able to replace some of the conventional thermochemical processes to obtain electrical energy.

It is necessary to study another kinds of coals and concentrations to evaluate and compare the performance of fuels with different characteristics and the solubility limits for each one.

The chemical analysis of the melts by means of infra-red, gas chromatograph or other analytical techniques to determine the possible composition and identities of electroactive organic species and gaseous products coupled to the high temperature fuel cell is necessary to increase the knowledge about the real system.

A better description of anode behaviour could be obtained if Electrochemical Impedance Spectroscopy is used as complementary technique to cyclic voltammetry. It could give information about reaction mechanisms and film formation over the surfaces. Also another techniques like TEM could be helpful to identify morphological, compositional and crystallographic characteristics of the electrode materials before and after the experimentation.

Bibliography

[1] Antoine Allanore. Electrochemical engineering of anodic oxygen evolution in molten oxides. *Electrochimica Acta*, 110:587–592, November 2013.

[2] Paulo E. Araya, Ricardo Badilla-Ohlbaum, and Sergio E. Droguett. Study of the treatment of subbituminous coals by NaOH solutions. *Fuel*, 60(12):1127–1130, December 1981.

[3] Yaohui Bai, Yan Liu, Yubao Tang, Yongmin Xie, and Jiang Liu. Direct carbon solid oxide Fuel Cell a potential high performance battery. *International Journal of Hydrogen Energy*, 36(15):9189–9194, July 2011.

[4] B Beverskog and I Puigdomenech. Revised Pourbaix diagrams for chromium al 25-300Â°C. *Corrosion Science*, 39(1):43–57, 1997.

[5] B Beverskog and I Puigdomenech. REVISED POURBAIX DIAGRAMS FOR NICKEL AT 25-300Â°C. *Corrosion Science*, 39(5):969–980, 1997.

[6] Dianxue Cao, Yong Sun, and Guiling Wang. Direct carbon fuel cell : Fundamentals and recent developments. *Journal of Power Sources*, 167:250–257, 2007.

[7] G A Carlson. Computer Simulation of the Molecular Structure of Bituminous Coal. *Energy & Fuels*, 6(6):771–778, 1992.

[8] Fidel Castro Marcano, Vladislav Lobodin V, Ryan P Rodgers, and Amy M McKenna. A molecular model for Illinois No 6 Argonne Premium coal: Moving toward capturing the continuum structure.pdf. *Fuel*, 95:35–49, 2012.

[9] Nerine J Cherepy, Roger Krueger, Kyle J Fiet, Alan F Jankowski, and John F Cooper. Direct Conversion of Carbon Fuels in a Molten Carbonate Fuel Cell. *Journal of Electrochemical Society*, 152:A80–A87, 2005.

[10] Paul Delahay. Theory of Irreversible Waves in Oscillographic Polarography. *Journal of the American Chemical Society*, 75(7):1190–1196, 1953.

[11] Frank Derbyshire, Anna Marzec, Hans-Rolf Schulten, Jean-Jaques Delpuech, Antoni Jurkievicz, Charles E Bronnimann, Robert A Wind, Gary E Maciel, Ramáni Narayan, Keith Bartle, and Colin Snape. Molecular structure of coals A debate.pdf. *Fuel*, 68:1091–1106, 1989.

[12] E Domalski. Selected values of heats of combustion and heats of formation of organic compounds containing the elements C, H, N, O, P and S. *Journal of Physical and Chemical Reference Data*, 1(2):221–277, 1972.

[13] Gumaa A El-nagar, Ahmad M Mohammad, Mohamed S El-deab, and Bahgat E El-anadouli. Facilitated Electro-Oxidation of Formic Acid at Nickel Oxide Nanoparticles Modified Electrodes. *Journal of The Electrochemical Society*, 159(7):249–254, 2012.

[14] Gumaa A El-nagar, Ahmad M Mohammad, Mohamed S El-deab, and Bahgat E El-anadouli. Electrocatalysis by design : Enhanced electrooxidation of formic acid at platinum nanoparticles at nickel oxide nanoparticles binary catalysts. *Electrochimica Acta*, 94:62–71, 2013.

[15] Jean-loup Faulon, Gary A Carlson, and Patrick G Hatcher. Statistical Models for Bituminous Coal : A Three-Dimensional Evaluation of Structural and Physical Properties Based on Computer-Generated Structures. *Energy & Fuels*, 7(6):1062–1072, 1993.

[16] Jean-Loup Faulon, Patrick G. Hatcher, Gary a. Carlson, and Kurt a. Wenzel. A computer-aided molecular model for high volatile bituminous coal. *Fuel Processing Technology*, 34(3):277–293, August 1993.

[17] S Giddey, S P S Badwal, a. Kulkarni, and C Munnings. A comprehensive review of direct carbon fuel cell technology. *Progress in Energy and Combustion Science*, 38(3):360–399, February 2012.

[18] M Greeff and M Toit. Looking at the Sensitization of 11-12% Chromium EN 1 . 4003 Stainless Steels during Welding. *Welding Journal*, 85(11):243–251, 2006.

[19] Biuck Habibi and Nasrin Delnavaz. Carbon-ceramic supported bimetallic Pt e Ni nanoparticles as an electrocatalyst for oxidation of formic acid. *International Journal of Hydrogen Energy*, 36(16):9581–9590, 2011.

[20] Jan Híveš, Michaela Benová, Karel Bouzek, and Virender K. Sharma. Electrochemical formation of ferrate(VI) in a molten NaOKOH system. *Electrochemistry Communications*, 8(11):1737–1740, November 2006.

[21] Sneh L. Jain, Yuta Nabae, Barry J. Lakeman, Kevin D. Pointon, and John T.S. Irvine. Solid state electrochemistry of direct carbon/air fuel cells. *Solid State Ionics*, 179(27-32):1417–1421, September 2008.

[22] Wei Jin, Michael S Moats, Shili Zheng, Hao Du, Yi Zhang, and Jan D Miller. Modulated Cr(III) oxidation in KOH solutions at a gold electrode: Competition between disproportionation and stepwise electron transfer. *Electrochimica Acta*, 56(24):8311–8318, October 2011.

[23] George Kapo and Calvert Seymour. Liquid phase oxidation of coal in alkali. *I&EC Process Design and Development*, 5(1):97–104, 1966.

[24] Xiang Li, Zhonghua Zhu, Jiuling Chen, Roland De Marco, Andrew Dicks, John Bradley, and Gaoqing Lu. Surface modification of carbon fuels for direct carbon fuel cells. *Journal of Power Sources*, 186:1–9, 2009.

[25] K Littlewood and M Monaghan. Carbonyl Groups in Bituminous Coals. *Nature*, 193:870–871, 1962.

[26] Zuzana Mácová, Karel Bouzek, and Virender K. Sharma. The influence of electrolyte composition on electrochemical ferrate(VI) synthesis. Part I: anodic dissolution kinetics of pure iron. *Journal of Applied Electrochemistry*, 40(5):1019–1028, December 2009.

[27] Juan M Marioli and Leonides E Sereno. The potentiodynamic behavior of nickel-chromium (80:20) alloy electrodes in 0.1N sodium hydroxide. *Electrochimica Acta*, 40(8):983–989, 1995.

[28] M H Miles. Exploration of molten hydroxide electrochemistry for thermal battery applications. *Journal of Applied Electrochemistry*, pages 1011–1016, 2003.

[29] Kazuo Nakamura. CAMD Study of Coal Model Molecules. 1. Estimation of physical Density of Coal Model Molecules. *Energy and Fuels*, 7(3):347–350, 1993.

[30] Tirdad Nickchi and Akram Alfantazi. Potential-temperature (ET) diagrams for iron , nickel , and chromium in sulfate solutions up to 473 K. *Electrochimica Acta*, 104:69–77, 2013.

[31] M Nishioka and B G Silbernagel. Evidence for charge-transfer complexes bituminous coal. *Fuel*, 70:341–348, 1991.

[32] Masaharu Nishioka and John W. Larsen. Association of aromatic structures in coals. *Energy & Fuels*, 4(1):100–106, January 1990.

[33] Teppei Nunoura, Kiyoshi Dowaki, Chihiro Fushimi, Stephen Allen, Erika Me, and Michael Jerry Antal. Performance of a First Generation , Aqueous Alkaline Biocarbon Fuel Cell. *Industrial & Engineering Chemistry Research*, 76:734–744, 2007.

[34] Kevin Pointon, Barry Lakeman, John Irvine, John Bradley, and Sneh Jain. The development of a carbon air semi fuel cell. *Journal of Power Sources*, 162(2):750–756, November 2006.

[35] William D Provine and Michael T Klein. MOLECULAR SIMULATION OF THERM L DIRECT COAL LIQUEFACTION. *Chemical Engineering Science*, 49(24):4223–4248, 1995.

[36] F Rosalbino, G Scavino, and M Actis Grande. Electrocatalytic activity of NiFeM (M = Cr , Mn , Cu) sintered electrodes for hydrogen evolution reaction in alkaline solution. *Journal of Electroanalytical Chemistry*, 694:114–121, 2013.

[37] Henry D Schreiber, Samuel J Kozak, G Bryan Balazs, L Ann, and W Charlotte. Equilibrium and Transport Properties of Gases in E-Glass Melts. *Journal of American Ceramics Society*, 72(9):1680–1691, 1989.

[38] Frank E. Senftle, Keith M. Patton, and Irvin Heard. Electrolytic oxidation of anthracite. *Fuel*, 60(12):1131–1136, December 1981.

[39] John Shinn. From coal to single-stage and two-stage products: a reactive model of coal structure.pdf. *Fuel*, 63:1187–1196, 1984.

[40] Toshimasa Takanohashi. Simulation of Interaction of Coal Associates with Solvents Using the Molecular Dynamics Calculation. *Energy & Fuels*, 12(15):1168–1173, 1998.

[41] Toshimasa Takanohashi. Computer Simulation of Methanol Swelling of Coal. *Energy & Fuels*, 13(4):922–926, 1999.

[42] Daniel Van Niekerk and Jonathan P. Mathews. Simulation of Solvent Extraction of South African Vitrinite- and Inertinite-Rich Coals. *Energy & Fuels*, 24(12):6393–6399, December 2010.

[43] Hans Werner Hoppe and Hans Henning Strehblow. XPS AND UPS EXAMINATIONS OF PASSIVE LAYERS ON NI AND FE53NI ALLOYS. *Corrosion Science*, 31:167–177, 1990.

[44] Strahinja Zecevic, Edward Patton, and Parviz Parhami. Direct Electrochemical Power Generation from Carbon in Fuel Cells with Molten Hydroxide Electrolyte. *Chemical engineering communications*, 192:37–41, 2005.

[45] Strahinja Zecevic, Edward M Patton, and Parviz Parhami. Carbon air fuel cell without a reforming process. *Carbon*, 42(10):1983–1993, January 2004.